Economic Geology, v. 113, no. 3, pp. 675–698

Petrogenesis and Ore Genesis of the Lengshuiqing Magmatic Sulfide Deposit in Southwest China: Constraints from Chalcophile Elements (PGE, Se) and Sr-Nd-Os-S Isotopes

Jun-Hua Yao,[1,2] Wei-Guang Zhu,[1,†] Chusi Li,[3] Hong Zhong,[1,2] Zhong-Jie Bai,[1] Edward M. Ripley,[3] and Chao Li[4]

[1]*State Key Laboratory of Ore Deposit Geochemistry, Institute of Geochemistry, Chinese Academy of Sciences, Guiyang 550081, China*

[2]*University of Chinese Academy of Sciences, Beijing 100049, China*

[3]*Department of Earth and Atmospheric Sciences, Indiana University, Bloomington, Indiana 47405, USA*

[4]*National Research Center for Geoanalysis, Beijing 100037, China*

Abstract

The Lengshuiqing magmatic Ni-Cu ore deposit is hosted in four small mid-Neoproterozoic mafic-ultramafic intrusions in the western margin of the Yangtze craton in China. The ore-bearing intrusions were emplaced into early Neoproterozoic metamorphosed volcanic-sedimentary rocks, granites, and diorites. The intrusions are dominated by lherzolite, olivine websterite, websterite, and gabbro, with sulfide mineralization associated with ultramafic rocks in the lower parts of the intrusions. The forsterite contents of olivine crystals in the Lengshuiqing ore-bearing intrusions are up to 86 mol %, indicating that their parental magma experienced moderate degrees of fractional crystallization. Olivine crystals in the intrusions are depleted in Ca (<1,000 ppm), a common feature for arc-type mafic-ultramafic intrusions worldwide. Moreover, clinopyroxene and Cr spinel in the Lengshuiqing ore-bearing mafic-ultramafic intrusions are remarkably similar to those in arc-type olivine-clinopyroxene cumulates elsewhere in the world. Whole-rock samples from these intrusions are all characterized by moderate light rare earth element (REE) enrichments relative to heavy REEs, moderate to significant degrees of negative Nb-Ta anomalies ($[Th/Nb]_N$ from 1.5–5), positive $\varepsilon_{Nd}(t)$ from 1.1 to 5.8, and low $(^{87}Sr/^{86}Sr)_i$ from 0.7038 to 0.7050. The isotope data indicate that the parental magma for these intrusions experienced only minor degrees of crustal contamination that cannot fully account for the observed negative Nb-Ta anomalies in the rocks. The data imply that the parental magmas were already depleted in Nb and Ta prior to crustal contamination. Taken together, the data support the view of an arc setting for the Lengshuiqing ore-bearing mafic-ultramafic intrusions. The occurrence of rare rounded sulfide inclusions in some olivine and spinel crystals in the intrusions indicates that immiscible sulfide droplets were present during olivine and spinel crystallization. Like most other arc-type magmatic sulfide deposits, the platinum group element (PGE) tenors of the Lengshuiqing deposit are very low. The estimated initial contents of PGEs in the parental magma of the Lengshuiqing deposit are two orders of magnitude lower than those in PGE undepleted picrites of continental flood basalt provinces such as the Emeishan and Siberian traps. The PGE depletions in the parental magma of the Lengshuiqing deposit are likely due to previous sulfide segregation during magma ascent or sulfide retention in the source mantle during partial melting. The $\delta^{34}S$, $\gamma_{Os}(t)$, and S/Se of the sulfide ores are from –4.0 to 1.3 ‰, from 115 to 320, and from 4,800 to 12,500, respectively. These values are significantly different from typical mantle values and indicate that addition of external sulfur played a major role in triggering sulfide saturation in the magma. The results from this study confirm that arc-type mafic-ultramafic intrusions are capable of hosting economically valuable magmatic Ni-Cu deposits and should be considered as part of global Ni exploration programs.

Introduction

The Lengshuiqing magmatic sulfide deposit is located in the western margin of the Yangtze craton in the northern part of the South China block (Fig. 1a). This deposit is one of several Neoproterozoic magmatic sulfide deposits that occur in cratonic margins in China (Fig. 1a). Examples include the Qingmingshan deposit in the southern margin of the Yangtze craton (848 ± 4 Ma; Zhou et al., 2017), the Xingdi deposit in the northern margin of the Tarim craton (737 ± 2 Ma; Han et al., 2016), and the Jinchuan deposit in the southwestern margin of the North China craton (831.8 ± 0.6 Ma; Zhang et al., 2010). Owing to its large size the Jinchuan deposit has been studied extensively in recent years (Duan et al., 2016, and references therein). In contrast, only a few studies of the small Lengshuiqing deposit have been carried out (Zhou et al., 2006; Zhu et al., 2007; Munteanu et al., 2010a, 2011). However, the interest in the Lengshuiqing deposit has increased as a result of a group of researchers proposing that the Lengshuiqing and Jinchuan deposits were related to the same mantle plume that was presumably centered beneath the Yangtze craton (X. Li et al., 2005, 2006). This hypothesis has significant implications not only for Rodinia reconstruction but also for Ni exploration in China (C. Li and Ripley, 2011). Thus, we have carried out a comparative study between the Lengshuiqing and Jinchuan deposits to evaluate this hypothesis.

The ages of the host intrusions of the Lengshuiqing deposit were determined previously using the zircon U-Pb method (Zhou et al., 2006; Munteanu et al., 2010b). Limited whole-rock chemical and Sr-Nd isotope data for the host intrusions were given in Zhou et al. (2006) and Zhu et al. (2007). The compositions of olivine and sulfide ores (Ni, Cu, platinum group element) in one of the mineralized mafic-ultramafic

†Corresponding author: e-mail, zhuweiguang@vip.gyig.ac.cn

ISSN 0361-0128; doi: 10.5382/econgeo.2018.4566; 24 p.
Supplementary files available online.

Submitted: November 10, 2017
Accepted: January 31, 2018

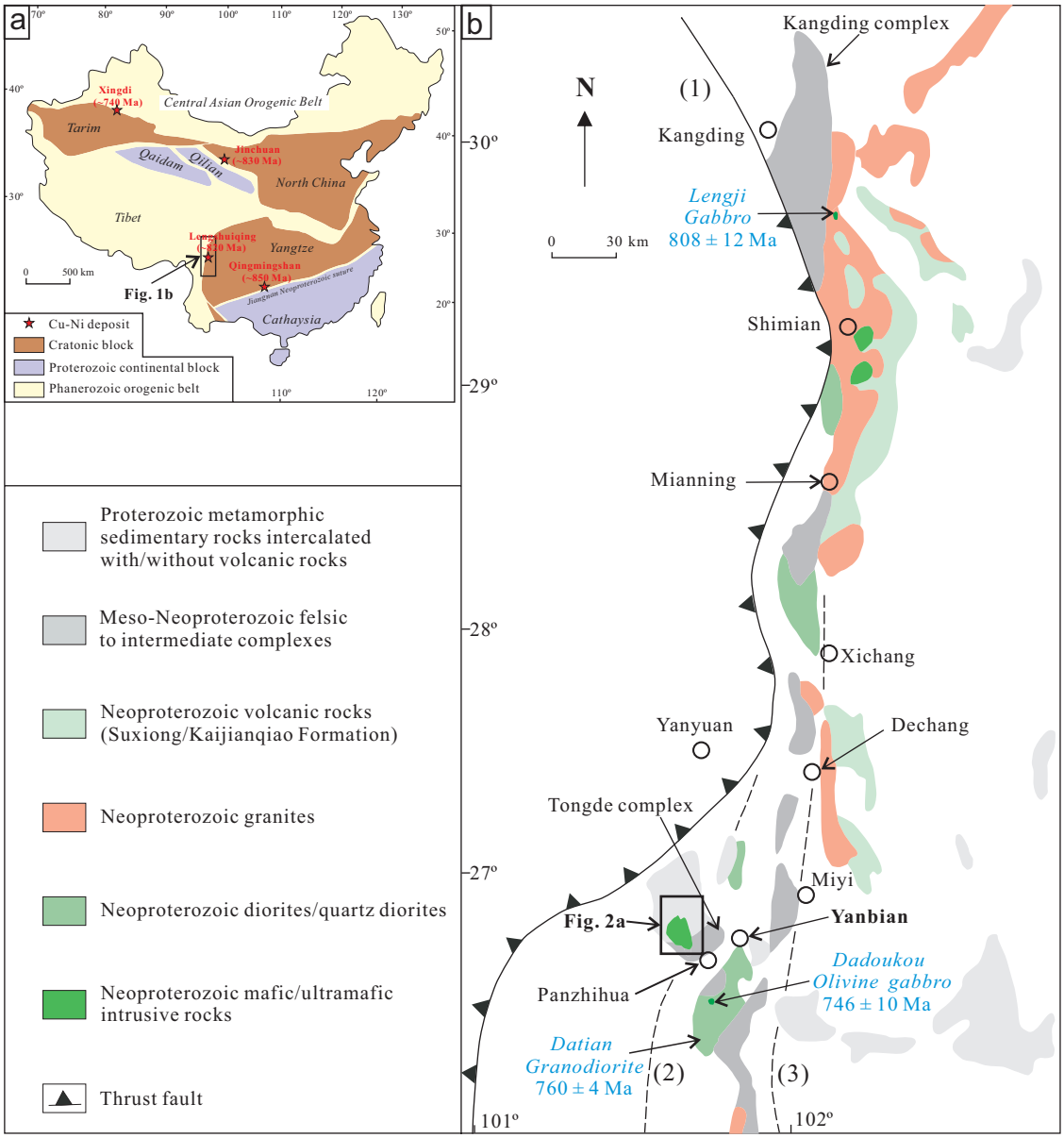

Fig. 1. (a) Schematic map showing the tectonic units of China and (b) schematic geologic map showing the Kangding-Panzhihua area, western South China, illustrating Neoproterozoic magmatic rocks and the basement (modified after Zhu et al., 2007). Symbols: (1) = Jinhe-Qinghe fault, (2) = Panzhihua fault, (3) = Xigeda fault. The zircon U-Pb isotope age data are from X. Li et al. (2002) and Zhao and Zhou (2007a, b).

intrusions (the interconnected I-II intrusion) were given in Munteanu et al. (2010a, b, 2011). In this paper we report additional data such as S-Os isotopes and S/Se ratios for the deposit, new platinum group element (PGE) data, systematic mineral compositions (Cr spinel, olivine, and clinopyroxene), and complementary whole-rock chemical and Sr-Nd isotope compositions for the other two mineralized intrusions (101 and III). These data, together with geologic constraints, are used to evaluate the competing geodynamic models (subduction vs. mantle plume) that have been proposed for the associated basaltic magmatism (X. Li et al., 2006; Munteanu et al., 2010a, 2011) as well as the fundamental controls on the genesis of this type of magmatic Ni-Cu ore deposit. The implications of the results from this study for Ni exploration at both global and regional scales are also discussed.

Geologic Background

The South China block consists of the Yangtze craton in the north and the Cathaysia block in the south (Fig. 1a). The Yangtze craton is separated from the North China craton by the late Paleozoic-early Mesozoic Qinling-Dabie orogenic belt to the north and is bounded by the Tibetan plateau to the west. The basement of the Yangtze craton is composed of Archean crystalline and high-grade metamorphic rocks, and its sedimentary cover is composed of post-Archean low-grade metamorphosed sedimentary sequences (Yan et al., 2003).

Abundant felsic to mafic metavolcanic rocks are interbedded within the Proterozoic strata that are exposed in the southern and western margins of the craton (Greentree et al., 2006; X. Li et al., 2006; Greentree and Li, 2008; Zhao et al., 2010). Numerous mafic-ultramafic intrusions with zircon U-Pb ages of 820 to 750 Ma are present in these areas (Zhou et al., 2002a, b; Z. Li et al., 2003). Neoproterozoic to Permian strata are mainly composed of clastic sedimentary rocks, carbonates, and metavolcanic rocks.

Abundant Neoproterozoic (860–740 Ma) intrusive rocks with compositions varying from granodiorites to mafic-ultramafic rocks are exposed in the western margin of the Yangtze craton from Kangding to Yanbian and Datian (Fig. 1b). In the Yanbian region where the Lengshuiqing deposit is located, numerous Neoproterozoic dolerite and picrite dikes have intruded the Early Neoproterozoic Yanbian Group and large diorite plutons (Fig. 2a; Electronic Supplement, Table A1). The Yanbian Group is mainly composed of volcanic-sedimentary rocks, such as pillow basalts, carbonaceous and tuffaceous slates, sandstones, and conglomerates, all of which have experienced greenschist-facies metamorphism. Two large subduction-related diorite plutons that intrude the Yanbian Group, the Guandaoshan pluton in the north and the Tongde pluton in the south, yield zircon U-Pb ages of ~860 Ma (Sun and Zhou, 2008) and ~825 Ma (Munteanu et al., 2010c), respectively (Fig. 2a). These data indicate that the Yanbian Group was deposited prior to 860 Ma, perhaps with the basal members deposited prior to 920 Ma (X. Li et al., 2006; Sun et al., 2008). The pillow basalts of the Yanbian Group show mid-ocean ridge basalt (MORB)-like geochemical characteristics and were thus thought to have formed in a rifted back-arc basin (X. Li et al., 2006). A consensus that has emerged from a decade-long debate is that the Yanbian region was an arc system from ~920 to ~825 Ma (e.g., X. Li et al., 2006; Zhou et al., 2006; Sun et al., 2007, 2008; Du et al., 2014). The younger age is defined by the presence of the ~825 Ma Tongde subduction-related diorite pluton in the region (Munteanu et al., 2010c). The origin of the younger Neoproterozoic mafic-ultramafic dikes and intrusions that were emplaced in the region between 824 and 796 Ma is still debated (Fig. 2a). Some researchers believe that they are mantle plume-related (e.g., X. Li et al., 2006; Zhu et al., 2006, 2007, 2008, 2010) whereas other researchers believe that they are subduction-related (e.g., Zhou et al., 2002a, b, 2006; Munteanu et al., 2010a, b). The main argument employed by the mantle-plume proponents is a temporal correlation between these intrusions and the ~827 Ma Gairdner Dyke Swarm in Australia that was thought to be of mantle plume origin. The same argument was previously proposed by Z. Li et al. (1999) to link the contemporaneous Neoproterozoic mafic-ultramafic intrusions in the southern margin of the Yangtze craton (Fig. 1a) to the Gairdner Dyke Swarm in Australia. The opponents of the mantle plume model emphasized the fact that the majority of the Neoproterozoic mafic-ultramafic intrusive rocks in the Yanbian region show arc-like geochemical characteristics. Such characteristics include depleted mantle-like Sr-Nd isotope compositions coupled with negative Nb-Ta anomalies that cannot be explained by very low degrees of crustal contamination (Zhou et al., 2006; Munteanu et al., 2010a, 2011). A few younger mafic-ultramafic dikes, such as the 796 Ma picrite dike situated north of Tongde (Zhu et al., 2010) and the 806 Ma dolerite dike located south of Yumen (Niu et al., 2015) show ocean island basalt (OIB)-like geochemical characteristics, similar to the compositions of the Permian Emeishan flood basalts (Munteanu et al., 2017). Based on this similarity and the fact that the Yanbian region is within the footprint of the Permian Emeishan large igneous province, Munteanu et al. (2017) suggested that the OIB-like dikes are feeders of the Permian flood basalts and that the Neoproterozoic zircon crystals in these dikes are xenocrysts that were able to survive because of rapid cooling in such small intrusions. Because these dikes are volumetrically insignificant it is difficult to extend genetic interpretations to the older (817–809 Ma) mafic-ultramafic intrusions in the region. In addition OIB-like mafic-ultramafic dikes are more common, but not unique, to a mantle plume. It is possible that different types of mantle-derived magmas that formed by different processes at similar times (e.g., subduction-related, plume-related, or rift-related) could be emplaced within the crust in close spatial proximity. It is important to note that a large, younger (~760 Ma), granodiorite pluton with arc characteristics (Zhao and Zhou, 2007b) is present immediately south of Yanbian (Fig. 1b); the presence of this pluton strongly supports the view that the western rim of the Yangtze craton was still an active continental margin at this time.

Geology of the Lengshuiqing Deposit and Sample Descriptions

The Lengshuiqing deposit contains ~30 million metric tonnes of ore with average grades of 0.76 wt % Ni and 0.27 wt % Cu (Zhu et al., 2007). The geology of the Lengshuiqing magmatic Ni-Cu sulfide deposit was described previously by Zhu et al. (2007) and Munteanu et al. (2010a, b, 2011). A brief description based on the previous studies is given below. The Lengshuiqing deposit comprises several orebodies hosted in four separate small mafic-ultramafic intrusions in a small area, numbered as I-II (interconnected at depth), III, IV, and 101 by mining geologists (Fig. 2b). The sizes of these intrusions vary from several to tens of meters in width and more than 100 m in length. The I-II, III, and IV intrusions are exposed on the surface. The 101 intrusion occurs ~150 m beneath the surface. The I-II intrusion is composed of ultramafic rocks (peridotites, pyroxenites) and mafic-intermediate rocks. The III intrusion is exclusively composed of ultramafic rocks. The IV intrusion is mainly composed of dioritic rocks, with minor peridotites and granites. The 101 intrusion has an irregular shape in cross section (Fig. 2c) and is divided into two zones: a gabbro zone and an olivine websterite zone. Sulfide mineralization mainly occurs within the olivine websterite zone and occasionally within the gabbro zone that occurs near the contact with the ultramafic rocks. A large sulfide-rich orebody occurs in the lower, eastern part of the 101 intrusion, with a length of ~100 m and thickness of ~80 m. The sulfide zone tends to bifurcate westward.

The samples used in this study were collected from two drill cores (ZK37801, ZK37802) of the 101 intrusion and a stockpile of sulfide ores from the III intrusion. Important ultramafic rocks associated with sulfide mineralization in these two intrusions are mainly lherzolite (Fig. 3a) and olivine websterite (Fig. 3b). In these rocks, olivine ± pyroxene occurs as cumulus

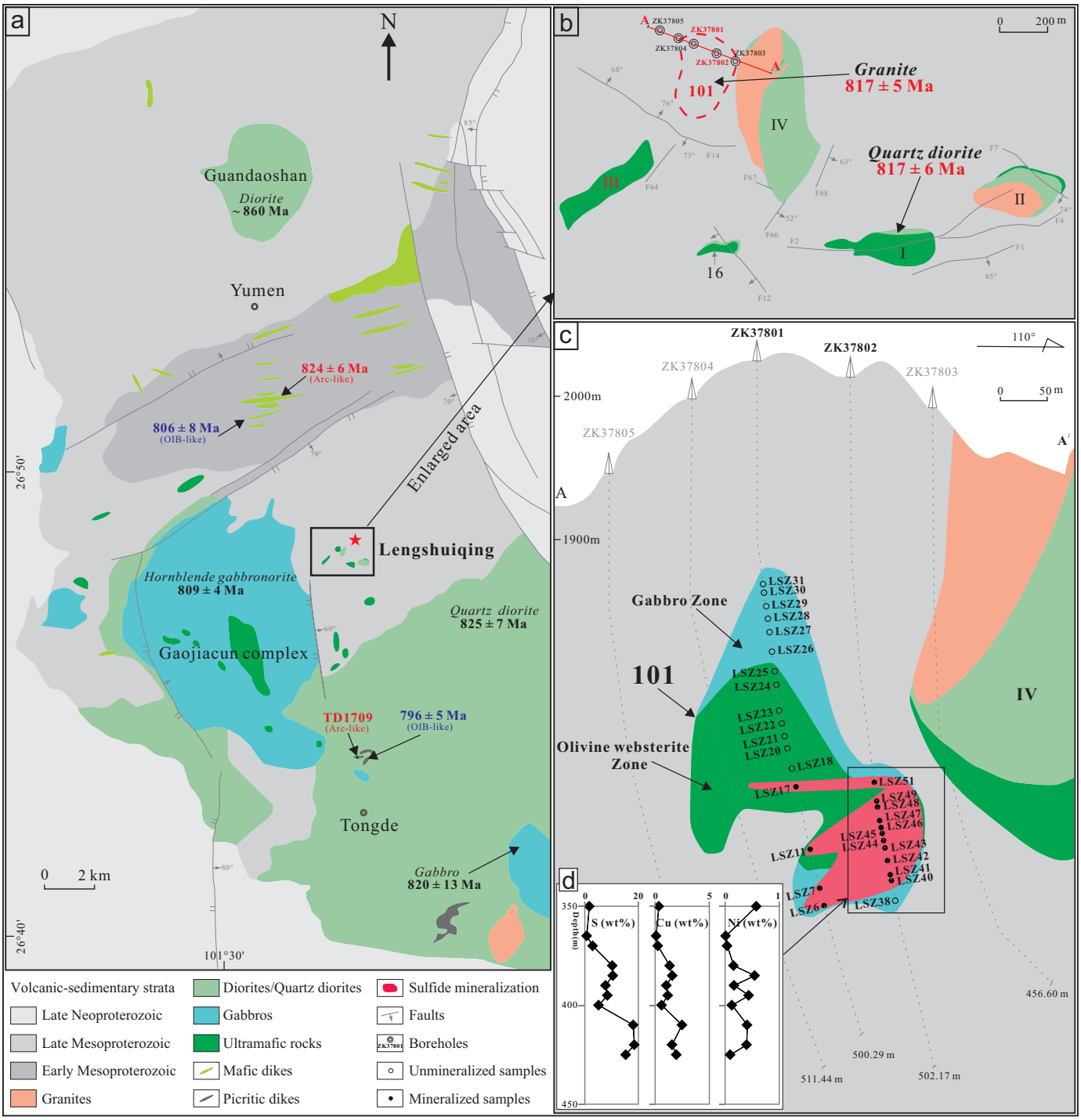

Fig. 2. (a) Simplified geologic map of the Yanbian region (Zhu et al., 2007) showing several dioritic intrusions and mafic-ultramafic intrusions and dikes with different ages (Electronic Supplement, Table A1); (b) simplified geologic map of the Lengshuiqing Cu-Ni sulfide deposit (modified after Zhu et al., 2007); (c) cross section and sampling sites on the borehole ZK37801 to borehole ZK37805 from the 101 intrusion in Lengshuiqing deposit; (d) Stratigraphic variations of S, Cu, and Ni (wt %) in ZK37802. OIB = ocean island basalt.

phases, and some clinopyroxene, hornblende, and phlogopite occur in the interstitial spaces. Variable degrees of hydrothermal alteration can be observed in the ultramafic rocks. Olivine is partially altered to serpentine plus secondary magnetite, orthopyroxene is variably replaced by talc, and clinopyroxene is partially altered to actinolite. The sulfide aggregates occur interstitially to grains of olivine and pyroxene. With increasing sulfide contents the type of sulfide mineralization is defined as disseminated, net-textured, and massive (Fig. 3c-e). The sulfide assemblage is mainly composed of pyrrhotite, pentlandite,

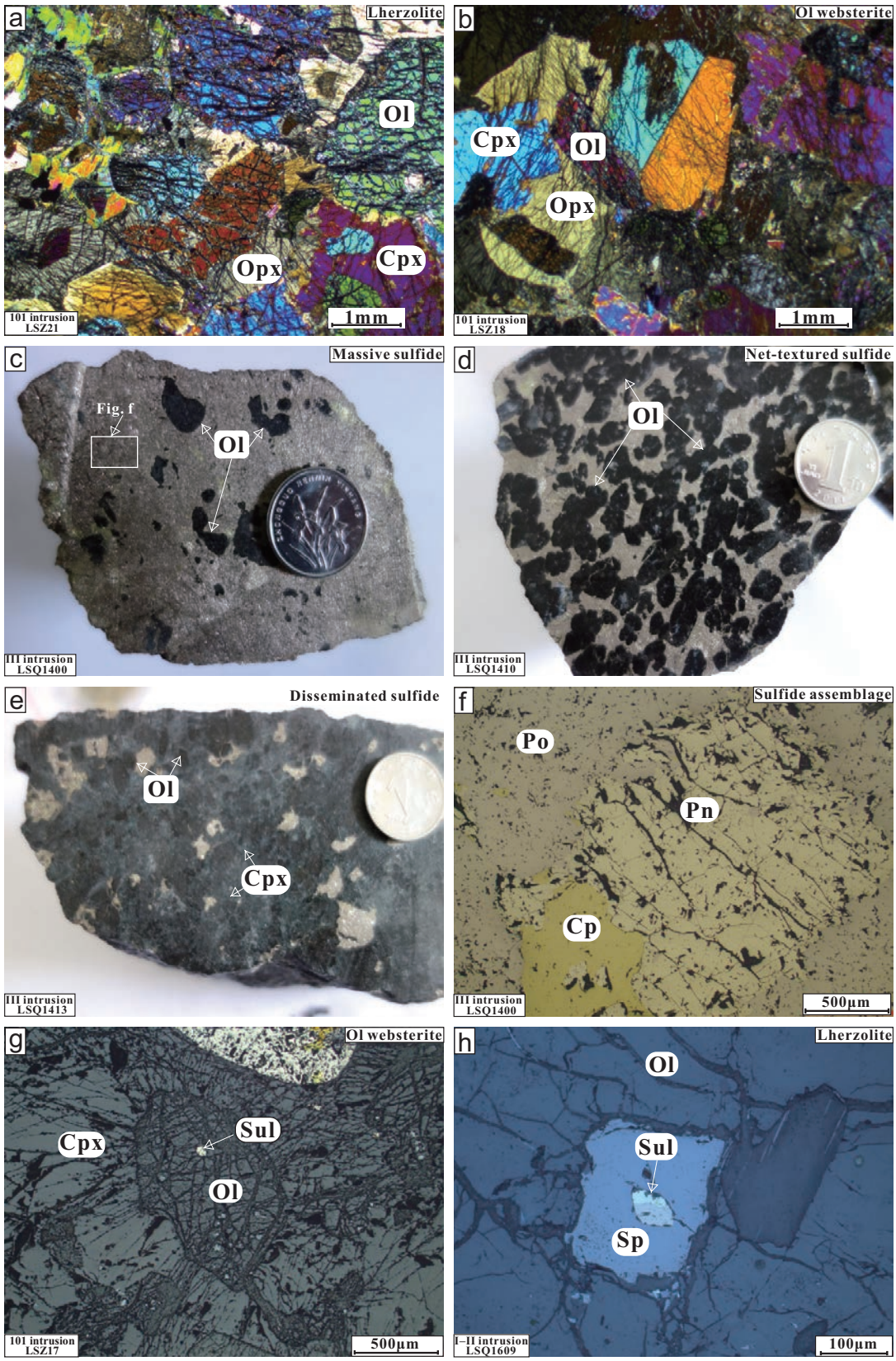

Fig. 3. Photographs of representative rocks and ores from the Lengshuiqing sulfide deposit: (a) lherzolite, (b) olivine websterite, (c) massive sulfide, (d) net-textured sulfide, (e) disseminated sulfide, (f) sulfide assemblage, (g) sulfide inclusion in olivine, and (h) sulfide inclusion in spinel. Mineral abbreviations: Cp = chalcopyrite, Cpx = clinopyroxene, Ol = olivine, Opx = orthopyroxene, Pn = pentlandite, Po = pyrrhotite, Sp = spinel, Sul = sulfide.

and chalcopyrite (Fig. 3f). Zhu et al. (2007) reported the presence of minor amounts of cobaltite, pyrite, sphalerite, hessite, and tsumoite. Pentlandite crystals are commonly subhedral grains, irregular segregations, and flames produced by immiscibility that are enclosed by anhedral or subhedral grains of pyrrhotite. Anhedral chalcopyrite grains generally occur between the other sulfides or enclosed by pyrrhotite. Small, rounded sulfide inclusions in olivine crystals (Fig. 3g) and Cr spinel crystals (Fig. 3h) are rare but have been found in a few samples.

Analytical Methods

Mineral chemical compositions were determined by wavelength-dispersive X-ray analysis using a JXA-8100 electron microprobe at Chang'an University, Xi'an, China. The analytical conditions were 20-nA beam current, 15-kV acceleration voltage, 1-μm diameter beam size, and 20- to 60-s counting times (Table 1). The concentrations of major elements, plus Cu and Ni, in whole rocks were determined using X-ray fluorescence (XRF) methods in the analytical laboratory of the ALS Chemex Co Ltd in Guangzhou, China. Certified reference materials (NIM-GBW07105, GBW07163, GBM908-10, MRGeo08) were used as the standards (Table 2). The analytical precision was estimated to be better than 5%. The concentrations of trace elements in whole rocks were determined using a Perkin-Elmer Sciex ELAN DRC-e inductively coupled plasma-mass spectrometer (ICP-MS) in the State Key Laboratory of Ore Deposit Geochemistry, Institute of Geochemistry, Chinese Academy of Sciences, Guiyang, China. Powdered samples (50 mg) were dissolved using HF + HNO_3 in high-pressure Teflon bombs at ~190°C for 48 h (Qi et al., 2000). Rh was used to monitor signal drift during ICP-MS analysis. International reference materials (BHVO-2, BCR-2) were used as the standards (Table 2). The analytical precision was estimated to be better than 10%. The contents of S and Se in whole rocks were measured using a LECO CS844 Carbon/Sulfur Analyzer and an Agilent 7700X ICP-MS, respectively, in the analytical laboratory of the ALS Chemex Co. Ltd in Guangzhou, China. Certified reference materials (GGC-04, GS310-8, OGGEO08) were used as the standards (Table 3). The analytical precisions were estimated to be 5% for S and ~10% for Se.

The concentrations of PGEs were determined by isotope dilution (ID)-ICP-MS following an improved digestion technique using sealed beakers in stainless steel pressure bombs (Qi et al., 2011). Powdered samples (3–5 g for massive and net-texture ores, 5–8 g for disseminated ores) were dissolved using HF in customized 120-ml PTFE beakers on a hot plate. The dried residues were then digested using HF + HNO_3 solution in stainless steel pressure bombs at 190°C for ~48 h. The solutions were analyzed using an ELAN DRC-e ICP-MS in the State Key Laboratory of Ore Deposit Geochemistry, Institute of Geochemistry, Chinese Academy of Sciences, Guiyang, China. The detection limits were estimated to be <0.02 ppb for Pt and Pd and <0.01 ppb for Ir, Ru, and Rh (Qi et al., 2011). International reference material WGB-1 and duplicate samples were analyzed together (Table 3).

Whole-rock powder samples for Sr-Nd isotope analyses were spiked and dissolved using HF-HNO_3-$HClO_4$ solution in Teflon bombs. The conventional cation exchange techniques were used for element separation. The isotope measurements were carried out using a Nu Plasma multicollector ICP-MS in the State Key Laboratory of Environmental Geochemistry, Institute of Geochemistry, Chinese Academy of Sciences, Guiyang, China. Mass fractionation correction for Sr and Nd isotope ratios were based on $^{86}Sr/^{88}Sr = 0.1194$ and $^{146}Nd/^{144}Nd = 0.7219$ (Nier, 1938; Wasserburg et al., 1981). The U.S. Geological Survey (USGS) rock standard BCR-2 was analyzed with our samples and yielded $^{87}Sr/^{86}Sr = 0.705134 \pm 16$ ($n = 3$, 2σ) and $^{143}Nd/^{144}Nd = 0.512637 \pm 12$ ($n = 3$, 2σ) (Table 4). These values are identical to the recommended values (http://georem.mpch-mainz.gwdg.de/sample_query_pref.asp).

Sulfur isotope analyses were carried out at Indiana University using the continuous-flow method of Studley et al. (2002). Sulfides were drilled under a microscope from polished sections using a 0.75-mm carbide drill bit. Between 0.1 and 0.2 mg of sulfide powder was placed in tin cups with approximately 1.5 to 2 mg vanadium pentoxide (V_2O_5). Samples were prepared in an elemental analyzer by flash combustion at 1,800°C with a reactor column temperature of 1,010°C. Measurements of produced SO_2 were made using a Finnigan Delta V stable isotope ratio mass spectrometer, with results reported in delta notation relative to Vienna-Canyon Diablo Troilite (V-CDT). Results are given in per mil designation via multiplication by 1,000 (Table 5). Analytical uncertainty was less than ±0.05‰. Sample reproducibility was ±0.2‰.

Re and Os isotopes were determined using a Triton-plus thermal ionization mass spectrometer in the National Research Center of Geoanalysis in Beijing, China, following the procedures given in Du et al. (2004). Os was separated as OsO_4 by distillation at 105° to 110°C and was trapped using Milli-Q water. Re was extracted from the residue using acetone in 5 M NaOH solution. ^{190}Os and ^{185}Re were used to correct the interference between Os and Re. The measured ratios were corrected for isobaric oxygen interferences and mass fractionation using the recommended $^{185}Re/^{187}Re = 0.59738$ and $^{192}Os/^{188}Os = 3.08271$ (Chao Li et al., 2015). Certified reference material (GBW04477) and duplicate samples were analyzed together (Table 6).

Analytical Results

Mineral compositions

The compositions of olivine, Cr spinel, clinopyroxene, and orthopyroxene from the Lengshuiqing intrusions are given in Table 1. Olivine crystals in the 101 and III intrusions contain 75 to 83 mol % forsterite (Fo = 100 Mg/[Mg + Fe], molar), 400 to 2,200 ppm Ni, 1,580 to 4,100 ppm Mn, and <400 ppm Ca. The forsterite contents of olivine in these intrusions are within the range of those for olivine in the I-II intrusion (75–86 mol %; Munteanu et al., 2010a, b). As shown in Figure 4a, the higher values of forsterite (81–86 mol %) in olivine of the Lengshuiqing deposit are similar to those that define the entire range of olivine compositions for the Jinchuan deposit (C. Li et al., 2004). In the Lengshuiqing deposit, more primitive olivine with forsterite >81 mol % are restricted to the sulfide-mineralized rocks (S content >0.5 wt %). Olivine crystals in the sulfide-barren samples (S content <0.5 wt %) have lower forsterite contents (76–81 mol %). A sulfide-barren

Table 1. Chemical Compositions of Minerals, Lengshuiqing Mafic-Ultramafic Intrusions

Olivine

Sample	Intrusion no.	Rock type	*n*	SiO_2	MgO	CaO	MnO	FeO	NiO	Total	Fo	Ca(ppm)	Ni(ppm)
LSQ1402	III	Websterite	5	39.13	41.07	0.01	0.41	19.47	0.23	100.32	79.0	100	1,800
LSQ1408	III	Ol websterite	5	38.18	40.26	0.02	0.48	20.68	0.14	99.77	77.6	116	1,134
LSQ1413	III	Lherzolite	5	38.58	41.12	0.01	0.28	20.08	0.16	100.23	78.5	100	1,236
LSQ1414	III	Ol websterite	7	38.13	40.62	0.02	0.37	20.24	0.12	99.50	78.1	160	920
LSZ11	101	Ol websterite	6	39.07	41.83	0.02	0.28	18.52	0.13	99.84	80.1	115	1,006
LSZ17	101	Lherzolite	6	39.20	42.25	0.02	0.27	18.46	0.17	100.36	80.3	123	1,303
LSZ18	101	Ol websterite	7	38.98	41.36	0.02	0.29	18.58	0.12	99.35	79.9	119	942
LSZ19	101	Lherzolite	3	38.57	39.79	0.02	0.31	21.39	0.13	100.21	76.8	134	1,004
LSZ20	101	Lherzolite	6	38.62	41.60	0.02	0.27	17.62	0.12	98.25	80.8	170	932
LSZ21	101	Lherzolite	6	38.49	42.35	0.02	0.24	18.66	0.12	99.87	80.2	108	904
LSZ22	101	Lherzolite	4	38.88	40.49	0.01	0.29	20.23	0.12	100.02	78.1	100	971
LSZ23	101	Lherzolite	6	38.61	40.90	0.03	0.27	20.05	0.10	99.96	78.4	215	776
LSZ41	101	Ol websterite	2	38.53	37.68	0.01	0.34	21.26	0.19	98.02	76.0	100	1,520
LSZ44	101	Ol websterite	1	39.94	38.81	0.01	0.40	21.07	0.27	100.51	76.7	100	2,106
LSZ45	101	Ol websterite	2	38.45	42.23	0.01	0.26	18.84	0.15	99.93	80.0	100	1,148
LSZ49	101	Ol websterite	4	39.42	41.85	0.01	0.30	17.91	0.16	99.65	80.6	100	1,278

Cr spinel inclusions within olivine crystals

Sample	Intrusion no.	Rock type	*n*	Cr_2O_3	MgO	Al_2O_3	MnO	NiO	TiO_2	Fe_2O_3	FeO	Total	Cr#	Mg#
LSZ17	101	Lherzolite	1	26.31	5.21	27.32	0.54	0.15	0.32	12.94	28.12	100.90	39.2	24.8
LSZ20	101	Lherzolite	3	25.65	5.18	26.21	0.41	0.07	0.39	13.90	27.84	99.65	39.8	24.9
LSZ21	101	Lherzolite	1	25.52	4.32	23.96	0.40	0.07	0.56	16.29	29.12	100.25	41.7	20.9
LSZ22	101	Lherzolite	2	25.18	4.26	23.98	0.46	0.12	0.49	16.40	28.89	99.78	41.4	20.8
LSZ23	101	Lherzolite	2	26.32	3.70	22.67	0.48	0.12	0.58	15.68	29.34	98.89	43.8	18.3

Clinopyroxene

Sample	Intrusion no.	Rock type	*n*	SiO_2	Cr_2O_3	MgO	Fe_2O_3	FeO	Na_2O	MnO	CaO	Al_2O_3	TiO_2	Total	Mg#
LSQ1402	III	Websterite	4	51.45	0.56	15.48	0.43	5.87	0.37	0.16	20.60	4.47	0.79	100.17	81.4
LSQ1406	III	Ol websterite	5	51.65	0.51	15.98	0.48	5.26	0.37	0.13	20.64	4.25	0.67	99.94	83.3
LSQ1408	III	Ol websterite	2	51.65	0.72	16.38	0.39	4.52	0.32	0.20	20.74	3.86	0.73	99.51	85.7
LSQ1414	III	Ol websterite	1	50.54	0.65	16.25	1.56	3.64	0.34	0.15	20.79	3.56	0.41	97.88	85.1
LSZ18	101	Ol websterite	2	51.61	0.81	16.53	0.37	5.35	0.39	0.17	19.76	4.15	0.59	99.75	83.8
LSZ20	101	Lherzolite	4	49.96	0.71	15.61	1.36	5.05	0.44	0.17	19.88	5.28	0.78	99.24	81.6
LSZ21	101	Lherzolite	1	47.80	0.59	14.47	2.49	4.48	0.46	0.12	20.03	5.97	1.17	97.57	79.3
LSZ22	101	Lherzolite	1	48.63	0.52	15.12	3.22	4.12	0.54	0.24	19.62	5.48	0.86	98.34	79.3
LSZ23	101	Lherzolite	2	49.93	0.74	15.58	1.08	5.11	0.39	0.17	20.01	5.62	0.86	99.47	82.0
LSZ44	101	Ol websterite	1	51.66	0.13	15.24	1.15	3.40	0.10	0.15	24.32	2.84	0.70	99.69	85.9
LSZ45	101	Ol websterite	2	51.04	0.25	15.59	0.77	5.71	0.36	0.19	20.41	4.62	0.59	99.65	81.3
LSZ46	101	Clinopyroxenite	2	52.05	0.56	16.89	0.86	4.81	0.41	0.20	19.99	3.66	0.44	99.86	84.3

Orthopyroxene

Sample	Intrusion no.	Rock type	*n*	SiO_2	TiO_2	Al_2O_3	Cr_2O_3	MgO	CaO	MnO	FeO	Na_2O	Total	Mg#
LSZ11	101	Ol websterite	5	53.63	0.27	3.23	0.02	28.66	1.30	0.21	11.75	0.04	99.11	81.3
LSZ17	101	Lherzolite	9	53.33	0.17	3.18	0.20	28.22	0.94	0.28	12.62	0.05	98.99	79.9
LSZ18	101	Ol websterite	3	52.84	0.19	3.85	0.17	27.98	1.25	0.25	12.53	0.04	99.10	79.9
LSZ19	101	Lherzolite	3	53.03	0.03	3.84	0.06	26.23	1.04	0.34	13.40	0.35	98.32	77.7
LSZ20	101	Lherzolite	2	54.22	0.23	2.53	0.26	29.05	1.55	0.21	11.18	0.03	99.26	82.2
LSZ21	101	Lherzolite	2	53.46	0.28	4.21	0.36	28.44	1.32	0.27	12.14	0.06	100.53	80.7
LSZ22	101	Lherzolite	1	53.29	0.46	4.42	0.34	28.27	1.15	0.30	12.78	0.02	101.04	79.8
LSZ23	101	Lherzolite	1	52.25	0.44	4.22	0.27	26.96	1.15	0.22	13.52	0.03	99.06	78.0
LSZ41	101	Ol websterite	4	52.45	0.33	3.87	0.22	27.30	1.16	0.28	12.80	0.04	98.44	79.2
LSZ49	101	Ol websterite	4	53.81	0.30	2.87	0.33	28.34	1.51	0.22	11.57	0.06	99.00	81.4

Notes: *n* = number of analysis; oxide in wt %, Fo in mol %; $Cr^{\#} = 100 \times Cr/(Cr + Al)$, molar; $Mg^{\#} = 100 \times Mg/(Mg+Fe^{total})$, molar. Abbreviations: Fo = forsterite, Ol = olivine

Table 2. Whole-Rock Major and Trace Element Compositions in the Lengshuiqing Intrusions and Mafic Dike in the Yanbian Region

	Lengshuiqing III intrusions							
Rock type	LSQ1401 Clinopyroxenite	LSQ1403 Clinopyroxenite	LSQ1404 Clinopyroxenite	LSQ1405 Clinopyroxenite	LSQ1411 Clinopyroxenite	LSQ1402 Websterite	LSQ1406 Ol websterite	LSQ1407 Ol websterite
SiO_2	50.83	49.98	50.51	50.37	50.52	51.38	47.60	47.72
TiO_2	0.96	0.73	0.73	0.69	0.74	0.75	0.60	0.59
Al_2O_3	6.69	5.49	5.11	7.76	8.39	4.94	4.10	4.27
Fe_2O_3	8.17	10.72	7.81	8.77	9.66	6.47	10.12	9.63
MnO	0.20	0.21	0.19	0.17	0.17	0.18	0.21	0.19
MgO	14.12	14.91	15.70	14.42	13.96	22.02	23.80	24.12
CaO	17.60	16.99	19.16	16.74	14.82	13.51	12.95	12.91
Na_2O	0.89	0.76	0.65	0.77	0.95	0.56	0.46	0.44
K_2O	0.47	0.16	0.09	0.24	0.69	0.13	0.10	0.08
P_2O_5	0.08	0.05	0.04	0.07	0.10	0.06	0.06	0.05
Total	100	100	100	100	100	100	100	100
Sc	52.3	68.8	66.0	64.4	45.7	60.9	57.3	64.2
V	176	198	180	168	153	155	130	141
Cr	1,267	2,175	2,462	1,542	1,610	1,470	1,638	1,721
Co	580	264	374	450	349	531	477	383
Ni	4,658	12,104	5,225	13,901	2,013	3,531	6,256	2,053
Cu	16,896	5,635	9,674	12,008	10,153	14,303	12,102	10,051
Zn	84.2	148	111	160	98.5	116	411	124
Ga	6.71	6.56	5.49	6.47	8.69	6.08	3.36	4.59
Rb	6.04	2.67	2.34	3.94	9.94	2.77	2.84	2.71
Sr	135	113	97.8	237	240	81.7	72.4	89.7
Y	11.9	10.6	9.50	9.62	14.3	9.32	6.30	7.74
Zr	42.1	39.9	29.3	31.9	38.5	36.2	28.0	24.9
Nb	1.10	1.13	0.87	0.90	1.41	1.18	0.69	0.93
Cs	0.10	0.12	0.08	0.09	0.23	0.24	0.56	0.61
Ba	146	39.6	70.4	70.8	165	42.8	43.2	47.4
La	4.09	3.27	2.29	2.52	5.71	2.52	2.12	2.24
Ce	12.7	10.1	7.72	8.14	15.5	7.49	6.74	7.42
Pr	1.82	1.68	1.42	1.15	2.32	1.47	1.20	1.08
Nd	9.77	9.29	7.44	8.45	11.3	6.53	7.00	6.55
Sm	2.65	2.69	1.85	1.64	2.63	2.04	2.08	1.72
Eu	1.14	0.88	0.67	0.77	1.01	0.63	0.65	0.93
Gd	2.54	2.70	1.49	1.85	3.16	1.84	1.51	1.88
Tb	0.50	0.41	0.27	0.32	0.47	0.25	0.25	0.29
Dy	2.20	2.16	1.95	1.39	2.46	2.21	1.41	1.50
Ho	0.53	0.47	0.35	0.41	0.45	0.52	0.31	0.25
Er	0.97	1.35	0.85	1.04	1.26	0.82	0.65	0.65
Tm	0.15	0.13	0.12	0.09	0.17	0.12	0.10	0.07
Yb	0.83	0.89	0.92	0.66	1.07	0.95	0.49	0.60
Lu	0.13	0.11	0.11	0.09	0.15	0.10	0.04	0.09
Hf	0.82	1.57	1.41	0.87	1.28	1.43	0.46	0.96
Ta	0.24	0.22	0.22	0.23	0.18	0.23	0.18	0.27
Pb	4.81	7.15	19.4	5.71	7.01	10.1	18.9	13.5
Th	0.64	0.50	0.48	0.60	0.63	0.57	0.60	0.53
U	0.09	0.10	0.05	0.04	0.19	0.02	0.05	0.11
S (wt %)	12.1	5.51	7.36	8.20	6.36	10.1	9.46	6.91
Se	25.1	9.40	11.3	15.1	11.0	19.8	16.5	11.2

	Lengshuiqing III intrusions						Mafic dike in Yanbian region
Rock type	LSQ1408 Ol websterite	LSQ1409 Ol websterite	LSQ1412 Ol websterite	LSQ1414 Ol websterite	LSQ1413 Lherzolite	LSQ1410 Dunite	TD1709 Dolerite dike
SiO_2	47.82	47.34	49.98	47.09	44.30	40.97	50.64
TiO_2	0.63	0.53	0.47	0.58	0.49	0.37	0.61
Al_2O_3	4.17	3.53	6.20	5.01	4.91	2.71	12.96
Fe_2O_3	9.55	9.53	8.33	11.18	13.39	16.16	9.92
MnO	0.21	0.19	0.19	0.17	0.21	0.26	0.20
MgO	23.28	26.30	25.75	24.13	30.33	37.31	13.44
CaO	13.74	12.10	8.27	10.78	5.74	1.66	10.19
Na_2O	0.45	0.38	0.50	0.73	0.37	0.29	1.66
K_2O	0.09	0.06	0.25	0.25	0.13	0.18	0.26
P_2O_5	0.05	0.04	0.06	0.10	0.12	0.09	0.11
Total	100	100	100	100	100	100	100
Sc	42.4	37.6	28.2	36.2	22.7	15.0	33.3
V	134	112	101	132	98.4	37.9	228
Cr	1,770	1,610	699	1,320	1,310	387	1,010
Co	330	331	299	115	263	719	46.9
Ni	1,302	1,318	1,302	1,380	1,742	3,044	175
Cu	7,906	8,094	7,379	565	5,092	18,939	17.2

Table 2. *(Cont.)*

	Lengshuiqing III intrusions						Mafic dike in Yanbian region	
Rock type	LSQ1408 Ol websterite	LSQ1409 Ol websterite	LSQ1412 Ol websterite	LSQ1414 Ol websterite	LSQ1413 Lherzolite	LSQ1410 Dunite	TD1709 Dolerite dike	
Zn	132	178	738	82.4	135	151	145	
Ga	5.35	4.31	5.95	6.14	6.19	2.61	13.5	
Rb	3.33	1.07	5.32	3.81	2.28	1.94	1.84	
Sr	86.9	75.7	175	145	157	64.9	314	
Y	10.4	7.81	6.84	10.3	7.72	2.94	10.9	
Zr	26.0	18.9	21.9	41.6	36.4	16.5	53.5	
Nb	0.53	0.54	0.62	1.37	1.27	0.92	1.95	
Cs	0.16	0.31	0.39	0.38	0.66	0.09	0.06	
Ba	24.7	14.0	66.8	90.9	28.6	31.8	125	
La	2.32	1.76	2.84	4.74	4.15	1.84	7.94	
Ce	7.65	6.01	7.95	11.0	9.70	3.52	17.2	
Pr	1.42	1.04	0.99	1.62	1.25	0.48	2.30	
Nd	7.65	5.38	5.43	8.08	6.42	2.30	10.1	
Sm	2.45	1.80	1.34	2.07	1.49	0.59	2.12	
Eu	0.65	0.70	0.49	0.77	0.50	0.20	0.85	
Gd	2.28	1.87	1.40	2.11	1.31	0.57	2.23	
Tb	0.31	0.26	0.18	0.31	0.21	0.07	0.31	
Dy	1.75	1.33	1.16	1.76	1.30	0.45	1.83	
Ho	0.35	0.25	0.20	0.33	0.20	0.07	0.38	
Er	0.91	0.71	0.70	0.93	0.65	0.26	1.16	
Tm	0.12	0.07	0.07	0.13	0.13	0.04	0.17	
Yb	0.76	0.59	0.55	0.77	0.63	0.29	1.05	
Lu	0.09	0.05	0.09	0.10	0.07	0.03	0.16	
Hf	0.98	0.63	0.54	1.24	0.98	0.45	1.37	
Ta	0.09	0.07	0.11	0.12	0.12	0.07	0.12	
Pb	18.5	7.35	11.6	5.96	2.15	14.0	1.31	
Th	0.16	0.19	0.30	0.53	0.39	0.17	1.02	
U	0.01	0.01	0.05	0.12	0.07	0.01	0.16	
S (wt %)	6.26	5.95	5.68		3.48	14.7		
Se	11.6	9.80	10.1		5.00	13.5		

Rock type	NIM-GBW07105[1] Expected	NIM-GBW07105 This study	NIM-GBW07105 This study	GBW07163[2] Expected	GBW07163 This study	GBW07163 This study	GBM908-10[3] Expected	GBM908-10 This study
SiO_2	44.60	44.20	44.80	47.90	47.40	47.20		
TiO_2	2.37	2.37	2.37	0.52	0.52	0.53		
Al_2O_3	13.85	13.90	14.00	11.20	11.10	11.15		
Fe_2O_3	13.40	13.35	13.35	11.65	11.50	11.60		
MnO	0.17	0.17	0.17	0.49	0.48	0.48		
MgO	7.77	7.70	7.72	1.39	1.29	1.29		
CaO	8.81	8.88	8.89	4.70	4.62	4.64		
Na_2O							2.90	2.87
K_2O	2.32	2.32	2.32	3.10	2.99	3.08		
P_2O_5	0.95	0.95	0.95	0.13	0.13	0.13		
total								
Sc								
V								
Cr								
Co								
Ni	141	141	134					
Cu	47.9	47.9	47.9	10,505	10,305	10,305		
Zn								
Ga								
Rb								
Sr								
Y								
Zr								
Nb								
Cs								
Ba								
La								
Ce								
Pr								
Nd								
Sm								
Eu								
Gd								
Tb								
Dy								

Table 2. *(Cont.)*

Rock type	NIM-GBW07105[1] Expected	NIM-GBW07105 This study	NIM-GBW07105 This study	GBW07163[2] Expected	GBW07163 This study	GBW07163 This study	GBM908-10[3] Expected	GBM908-10 This study
Ho								
Er								
Tm								
Yb								
Lu								
Hf								
Ta								
Pb								
Th								
U								
S (wt %)	0.008	0.012	0.016	6.75	6.75	6.75		
Se								

Rock type	MRGeo08[4] Expected	MRGeo08 This study	BHVO-2[5] Expected	BHVO-2 This study	BHVO-2 This study	BCR-2[5] Expected	BCR-2 This study	BCR-2 This study
SiO_2								
TiO_2								
Al_2O_3								
Fe_2O_3								
MnO								
MgO								
CaO								
Na_2O	2.66	2.64						
K_2O								
P_2O_5								
total								
Sc			32	28.6	29.2	33	31.9	32.2
V			317	276	285	416	226	346
Cr			280	255	247	18	20.0	19.7
Co			45	42.6	42.9	37	36.2	36.4
Ni			119	112	113	18	31.5	14.5
Cu			127	121	122	21	27.0	27.7
Zn			103	131	133	127	154	154
Ga			22	20.7	20.9	23	21.7	21.3
Rb			9.11	10.5	10.3	46.9	49.5	50.0
Sr			396	449	441	340	379	379
Y			26	25.3	25.6	37	34.0	34.0
Zr			172	197	196	184	213	212
Nb			18.1	17.8	17.5	12.6	12.3	12.2
Cs			0.1	0.09	0.11	1.1	1.19	1.16
Ba			131	164	162	677	776	754
La			15.2	18.1	17.6	24.9	28.2	28.2
Ce			37.5	45.1	43.4	52.9	60.0	59.5
Pr			5.35	5.85	5.75	6.7	7.54	7.35
Nd			24.5	26.4	25.6	28.7	29.5	29.8
Sm			6.07	6.47	6.92	6.58	7.01	6.77
Eu			2.07	2.36	2.31	1.96	2.01	2.12
Gd			6.24	6.30	6.50	6.75	6.69	6.79
Tb			0.92	1.03	1.02	1.07	1.13	1.17
Dy			5.31	5.34	5.31	6.41	6.33	6.30
Ho			0.98	1.05	1.03	1.28	1.37	1.37
Er			2.54	2.62	2.67	3.66	3.66	3.77
Tm			0.33	0.36	0.32	0.54	0.58	0.53
Yb			2	2.02	1.99	3.38	3.49	3.31
Lu			0.274	0.30	0.28	0.503	0.55	0.53
Hf			4.36	4.76	4.69	4.9	5.18	5.00
Ta			1.14	1.38	1.27	0.74	0.88	0.83
Pb			1.6	1.50	1.59	11	11.0	11.0
Th			1.22	1.28	1.28	5.7	6.11	6.00
U			0.403	0.47	0.46	1.69	1.76	1.74
S (wt %)								

Notes: oxides and S in wt %; trace elements in ppm
Abbreviations: Ol = olivine
[1] Expected data of the NIM-GBW07105 are from https://www.lgcstandards.com/
[2] Expected data of the GBW07163 are from http://www.ncrm.org.cn/
[3] Expected data of the GBM908-10 are from http://www.geostats.com.au/
[4] Expected data of the MRGeo08 are from http://www.ore.com.au/
[5] Expected data of the BHVO-2, BCR-2 are from http://georem.mpch-mainz.gwdg.de/sample_query_pref.asp

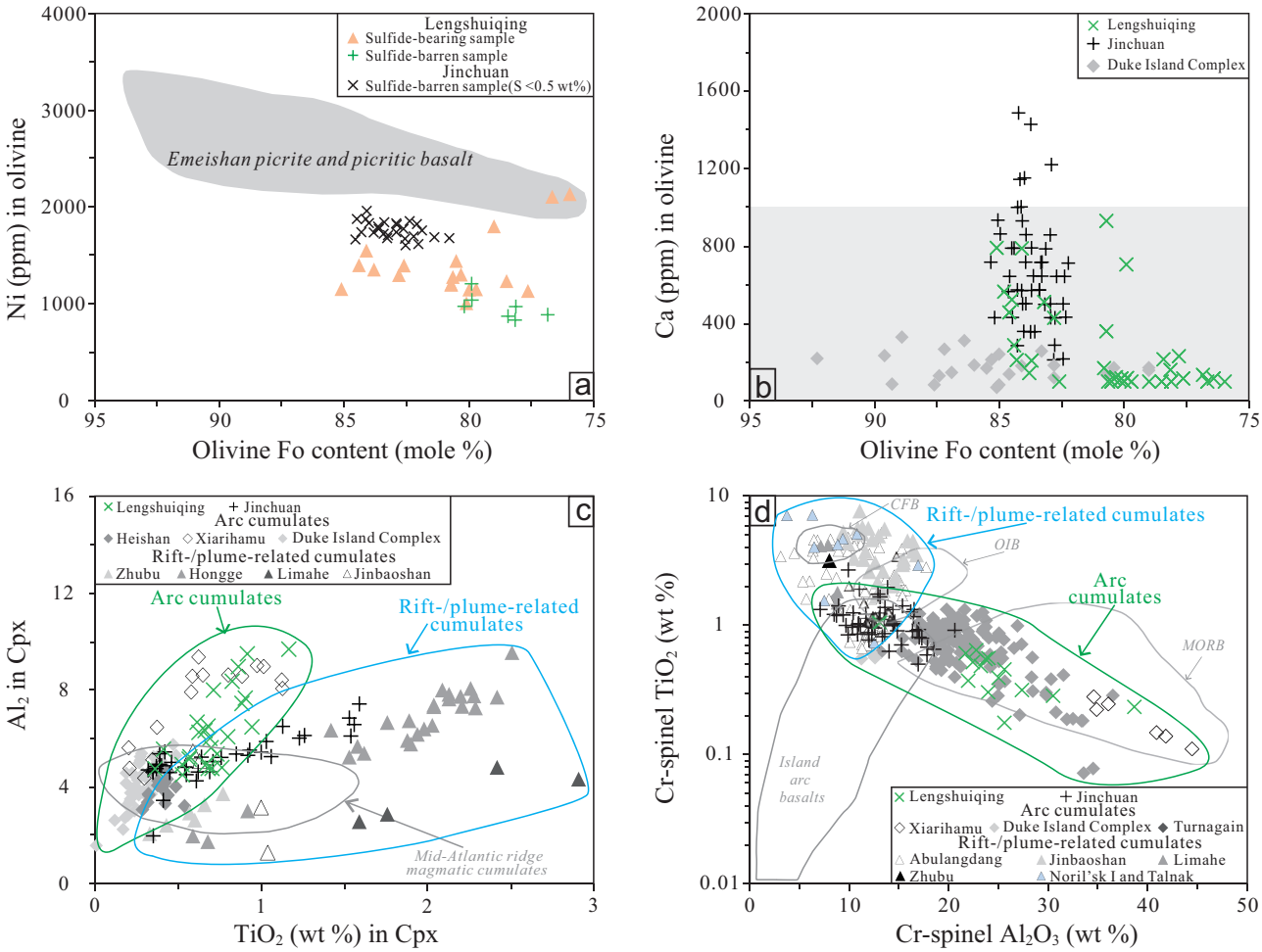

Fig. 4. Comparisons of the compositions of silicate minerals (olivine, clinopyroxene, and Cr spinel) in Lengshuiqing and Jinchuan deposits. (a) Average Ni forsterite in olivine. (b) Average Ca forsterite in olivine. (c) Al_Z-TiO_2 in clinopyroxene. Al_Z is the percentage of the tetrahedral site occupied by Al (Le Bas, 1962). Cpx is clinopyroxene. The field of Mid-Atlantic ridge magmatic cumulates are from Loucks (1990). (d) TiO_2 vs. Al_2O_3 contents in Cr spinel. The fields for continental flood basalts (CFB), ocean island basalts (OIB), mid-ocean ridge basalts (MORB) and island arc basalts in spinel are from Kamenetsky et al. (2001). Data for Emeishan are from C. Li et al. (2016). Data for Jinchuan are from Barnes and Tang (1999), C. Li et al. (2004), Chen et al. (2009), and Tonnelier, (2010). Data for Lengshuiqing are from this study and Munteanu et al. (2010a, b). Data for rift-/plume-related cumulates are from Barnes and Kunilov (2000) (Noril'sk I and Talnakh), Wang et al. (2005, 2014) (Jinbaoshan, Abulangdang), Tao et al. (2007, 2008) (Jinbaoshan, Limahe), Bai et al. (2012) (Hongge), and Tang et al. (2013) (Zhubu); data for arc cumulates are from Thakurta et al. (2008) (Duke Island Complex), Scheel et al. (2009) (Turnagain), Xie et al. (2012) (Heishan), and Chusi Li et al. (2015a) (Xiarihamu).

olivine websterite sample from the 101 intrusion (LSZ49) shows high variation in olivine forsterite contents from 78 to 83 mol %. Olivine crystals in the sulfide-barren samples exhibit a weak positive forsterite and Ni correlation, consistent with the combined effects of fractional crystallization and reequilibration with interstitial silicate melt (C. Li et al., 2007). The Ni contents of olivine crystals in the sulfide-mineralized samples, especially those with lower forsterite contents, are highly scattered and consistent with variable degrees of olivine-sulfide Fe-Ni exchange reactions (C. Li et al., 2007). As shown in Figure 4b, Olivine crystals in the Lengshuiqing 101 and III intrusions are all depleted in Ca (i.e., <1,000 ppm Ca), which is common for arc-type basalts and mafic-ultramafic intrusions worldwide (i.e., Kamenetsky et al., 2006; C. Li et al., 2012). In contrast, only some of the olivine crystals in the Jinchuan intrusion show Ca depletion (Fig. 4b).

The $Mg^{\#}$ (100 Mg/[Mg + Fe^{total}], molar) of clinopyroxene crystals in the ultramafic rocks of the 101 and III intrusions vary from 79 to 87. In a plot of Al_Z (100 Al^{IV} / [Al^{IV} + Al^{VI}]) vs. TiO_2 contents (Fig. 4c), clinopyroxene crystals of the Lengshuiqing intrusions plot within the field for arc cumulates as defined by intrusions such as the Heishan mafic-ultramafic intrusion in the southern margin of the Central Asian orogenic belt in northern Xinjiang (Xie et al., 2012), the Xiarihahu mafic-ultramafic intrusion in the Qinghai-Tibet plateau (Chusi Li et al., 2015a), and the Duke Island mafic-ultramafic complex in southern Alaska (Thakurta et al., 2008). In contrast, clinopyroxene crystals of the Jinchuan intrusion plot in the field for rift- or plume-related cumulates such as the Hongge, Jinbaoshan, Limahe, and Zhubu mafic-ultramafic intrusions in the Permian Emeishan large igneous province (Tao et al., 2007, 2008; Bai et al., 2012; Tang et al., 2013).

Table 3. Concentrations of Chalcophile Elements in the Lengshuiqing Intrusions

Sample	Intrusion no.	Rock type	S (wt %)	Ni (wt %)	Cu (wt %)	Ir (ppb)	Ru (ppb)	Rh (ppb)	Pt (ppb)	Pd (ppb)	Se (ppm)
LSZ6	101	Gabbro	7.32	1.11	1.02	0.08	0.09	0.10	0.84	21.8	9.8
LSZ7	101	Gabbro	3.54	0.40	0.15	0.02	0.16	0.07	0.37	19.3	5.6
LSZ11	101	Ol websterite	2.67	0.21	0.13	0.24	0.30	0.21	1.39	6.86	4.2
LSZ17	101	Lherzolite	11.5	1.94	0.40	1.37	2.07	1.24	0.50	15.5	13.7
LSZ40	101	Ol websterite	15.3	1.96	0.10	0.70	0.98	0.86	3.28	85.2	20.3
LSZ41	101	Ol websterite	13.7	1.56	0.40	1.49	1.87	1.57	1.61	14.7	14.3
LSZ42	101	Lherzolite	18.1	2.48	0.41	1.65	1.59	1.59	b.d.l.	32.8	23.1
LSZ43	101	Clinopyroxenite	5.17	0.60	0.13	0.64	0.98	0.87	1.09	7.51	7.4
LSZ44	101	Ol websterite	8.40	1.18	0.44	0.14	0.42	0.19	b.d.l.	10.7	13.7
LSZ45	101	Clinopyroxenite	7.81	1.05	0.17	0.11	0.24	0.21	0.33	10.8	13.4
LSZ46	101	Ol websterite	10.5	1.58	0.55	1.08	1.00	1.30	0.35	11.1	11.8
LSZ47	101	Websterite	10.3	1.35	0.16	1.07	1.49	0.61	0.20	6.09	8.2
LSZ48	101	Ol websterite	2.97	0.26	0.04	0.21	0.37	0.21	0.14	4.79	3.0
LSZ51	101	Ol websterite	1.67	0.34	0.58	0.03	0.09	0.02	5.46	39.8	5.8
LSQ1401	III	Clinopyroxenite	12.1	1.68	0.47	0.71	0.93	0.59	34.9	29.6	25.1
LSQ1402	III	Websterite	10.1	1.42	0.35	0.41	0.61	0.33	0.41	10.8	19.8
LSQ1403	III	Clinopyroxenite	5.51	0.55	1.21	0.13	0.41	0.14	62.6	12.7	9.4
LSQ1404	III	Clinopyroxenite	7.36	0.96	0.52	0.24	0.33	0.36	1.38	22.7	11.3
LSQ1405	III	Clinopyroxenite	8.20	1.19	1.39	0.19	0.21	0.26	20.6	51.3	15.1
LSQ1406	III	Ol websterite	9.46	1.20	0.63	0.18	0.27	0.29	0.20	16.7	16.5
LSQ1407	III	Ol websterite	6.91	1.00	0.21	0.20	0.25	0.35	0.55	13.9	11.2
LSQ1408	III	Ol websterite	6.26	0.77	0.13	0.14	0.24	0.17	0.80	7.46	11.6
LSQ1409	III	Ol websterite	5.95	0.79	0.13	0.07	0.12	0.18	0.64	9.92	9.8
LSQ1410	III	Dunite	14.7	1.83	0.30	1.99	2.65	0.69	9.23	45.6	13.5
LSQ1411	III	Clinopyroxenite	6.36	1.02	0.20	0.48	0.62	0.52	6.21	32.4	11.0
LSQ1412	III	Ol websterite	5.68	0.73	0.13	0.23	0.28	0.27	0.61	8.93	10.1
LSQ1413	III	Lherzolite	3.48	0.50	0.17	0.09	0.19	0.16	15.3	12.4	5.0
LSQ1413[1]						0.09	0.12	0.14	20.3	12.9	
GGC-04		Expected[2]	0.05								
		This study	0.04								
GS310-8		Expected[2]	5.91								
		This study	5.99								
OGGEO08		Expected[3]									11.1
		This study									11.2
		This study									11.3
		This study									10.3
		This study									11.0
WGB-1		Expected[4]				0.27 ± 0.03	0.15 ± 0.02	0.18 ± 0.02	4.95 ± 0.52	11.8 ± 0.8	
		This study				0.26	0.21	0.17	4.42	14.6	

Abbreviations: b.d.l. = below detection limit, Ol = olivine

[1] Duplicate samples

[2] Expected data of the GGC-04, GS310-8 are from http://www.geostats.com.au/

[3] Expected data of the OGGEO08 are from http://www.ore.com.au/

[4] Expected data of the WGB-1 are from Qi et al., 2011

Table 4. Sr-Nd Isotope Compositions of the Lengshuiqing Intrusions

Sample	Intrusion no.	Rock type	Rb (ppm)	Sr (ppm)	$^{87}Sr/^{86}Sr$ (2σ)	$(^{87}Sr/^{86}Sr)_i$	Sm (ppm)	Nd (ppm)	$^{143}Nd/^{144}Nd$ (2σ)	$(^{143}Nd/^{144}Nd)_i$	$\varepsilon_{Nd}(t)$
LSZ26	101	Gabbro	7.01	325	0.705756 (11)	0.70502	3.62	12.5	0.512576 (8)	0.51163	1.06
LSZ31	101	Gabbro	30.1	504	0.706435 (9)	0.70441	2.98	10.8	0.512545 (6)	0.51165	1.33
LSZ9	101	Gabbro	2.33	231	0.704421 (10)	0.70408	6.41	28.7	0.512497 (8)	0.51177	3.73
LSZ38	101	Clinopyroxenite	14.4	361	0.705475 (8)	0.70412	6.22	25	0.512554 (6)	0.51170	3.23
LSZ7	101	Gabbro	22.7	1094	0.704806 (9)	0.70410	8.48	44.2	0.512410 (6)	0.51179	4.03
LSZ51	101	Ol websterite	1.09	147	0.704538 (6)	0.70429	2.92	11.8	0.512564 (6)	0.51176	3.51
LSZ19	101	Lherzolite	20.7	223	0.706983 (7)	0.70383	1.86	9.21	0.512362 (10)	0.51171	2.46
LSZ22	101	Lherzolite	4.86	183	0.705101 (6)	0.70420	2.06	8.16	0.512520 (6)	0.51170	2.34
LSZ43	101	Clinopyroxenite	6.45	168	0.705520 (11)	0.70422	4.8	21.2	0.512416 (10)	0.51168	1.95
LSZ48	101	Ol websterite	7.15	152	0.705783 (10)	0.70419	1.84	7.95	0.512468 (6)	0.51172	2.66
LSZ48[1]	101	Ol websterite	7.15	152	0.705817 (9)	0.70422	1.84	7.95	0.512468 (8)	0.51172	2.66
LSQ1411	III	Clinopyroxenite	9.94	240	0.705555 (7)	0.70415	2.63	11.3	0.512635 (8)	0.51188	5.83
LSQ1414	III	Ol websterite	4.46	176	0.705354 (10)	0.70449	1.96	7.94	0.512570 (14)	0.51177	3.67
BCR-2		Expected[2]			0.70492				0.512635		
		This study			0.705126				0.512635		
		This study			0.705146				0.512646		
		This study			0.705131				0.512632		

Chondrite uniform reservoir (CHUR) values ($^{87}Rb/^{86}Sr = 0.0847$, $^{87}Sr/^{86}Sr = 0.7045$, $^{147}Sm/^{144}Nd = 0.1967$, $^{143}Nd/^{144}Nd = 0.512638$) are used for the calculation; $\lambda_{Rb} = 1.42 \times 10^{-11}$year^{-1} (Steiger and Jäger, 1977); $\lambda_{Sm} = 6.54 \times 10^{-12}$year^{-1} (Lugmair and Harti, 1978); the $(^{87}Sr/^{86}Sr)_i$, $(^{143}Nd/^{144}Nd)_i$, and $\varepsilon_{Nd}(t)$ of the Lengshuiqing intrusions were calculated using age of 817 Ma

Abbreviations: Ol = olivine

[1] Duplicate samples

[2] Expected data of the BCR-2 are from http://georem.mpch-mainz.gwdg.de/sample_query_pref.asp

Table 5. S Isotopes for the Lengshuiqing Magmatic Ni-Cu Ore Deposit

Sample	Rock type	Intrusion no.	$\delta^{34}S$ (‰)
LSQ1401	Clinopyroxenite	III	0.45
LSQ1402	Websterite	III	0.11
LSQ1403	Clinopyroxenite	III	–0.83
LSQ1404	Clinopyroxenite	III	1.02
LSQ1405	Clinopyroxenite	III	–0.98
LSQ1406	Ol websterite	III	0.03
LSQ1407	Ol websterite	III	0.47
LSQ1408	Ol websterite	III	–0.04
LSQ1409	Ol websterite	III	0.17
LSQ1410	Dunite	III	1.34
LSQ1411	Clinopyroxenite	III	–3.98
LSQ1412	Ol websterite	III	0.13
LSQ1413	Lherzolite	III	1.12

Abbreviations: Ol = olivine

Small Cr spinel inclusions enclosed in olivine crystals of the 101 and III intrusions contain on average ~26 wt % Cr_2O_3 and ~25 wt % Al_2O_3, with (100 Cr/[Cr + Al], molar) = ~40. As shown in Figure 4d, the Lengshuiqing Cr spinel crystals plot within the field for arc cumulates as defined by the Xiarihahu mafic-ultramafic intrusion in the Qinghai-Tibet plateau (Chusi Li et al., 2015a), the Duke Island mafic-ultramafic complex (Thakurta et al., 2008), and the Turnagain mafic-ultramafic complex in Alaska (Scheel et al., 2009). In contrast, Cr spinel crystals in the Jinchuan ultramafic intrusion plot in the field for rift- or plume-related cumulates as defined by the Abulangdang, Jinbaoshan, Limahe, and Zhubu mafic-ultramafic intrusions of the Emeishan large igneous province (Wang et al., 2005, 2014; Tao et al., 2008; Tang et al., 2013) and the Noril'sk I and Talnakh mafic-ultramafic intrusions of the Permian Siberian large igneous province (Barnes and Kunilov, 2000).

Major and trace elements in whole rocks

Whole-rock major and trace element compositions of samples from the III mafic-ultramafic intrusions are listed in Table 2. A comparison with the compositions of constituent minerals is illustrated in Figure 5. In the comparison the normalized 100% anhydrous silicate compositions (free of loss-on-ignition and base metal sulfide) are used. The amounts of sulfide minerals (pyrrhotite + pentlandite + chalcopyrite) in the samples were estimated using whole-rock S and Cu contents and corrected Ni contents (free of Ni from olivine) using the procedures given in C. Li et al. (2001). The comparison reveals that the abundances of major oxides in the ultramafic rocks and gabbros are mainly controlled by the abundances of olivine + pyroxene and clinopyroxene + plagioclase, respectively, which are consistent with cumulate origins for these rocks.

The chondrite-normalized rare earth element (REE) patterns of the sulfide-barren samples from the Lengshuiqing mafic-ultramafic intrusions are illustrated in Figure 6a. The patterns are remarkably similar to that of a coeval dolerite dike in the area, showing enrichments in light REEs relative to heavy REEs. However, the abundances of all REEs in the Lengshuiqing samples from the olivine websterite zone are significantly lower than those in the dolerite dike, consistent

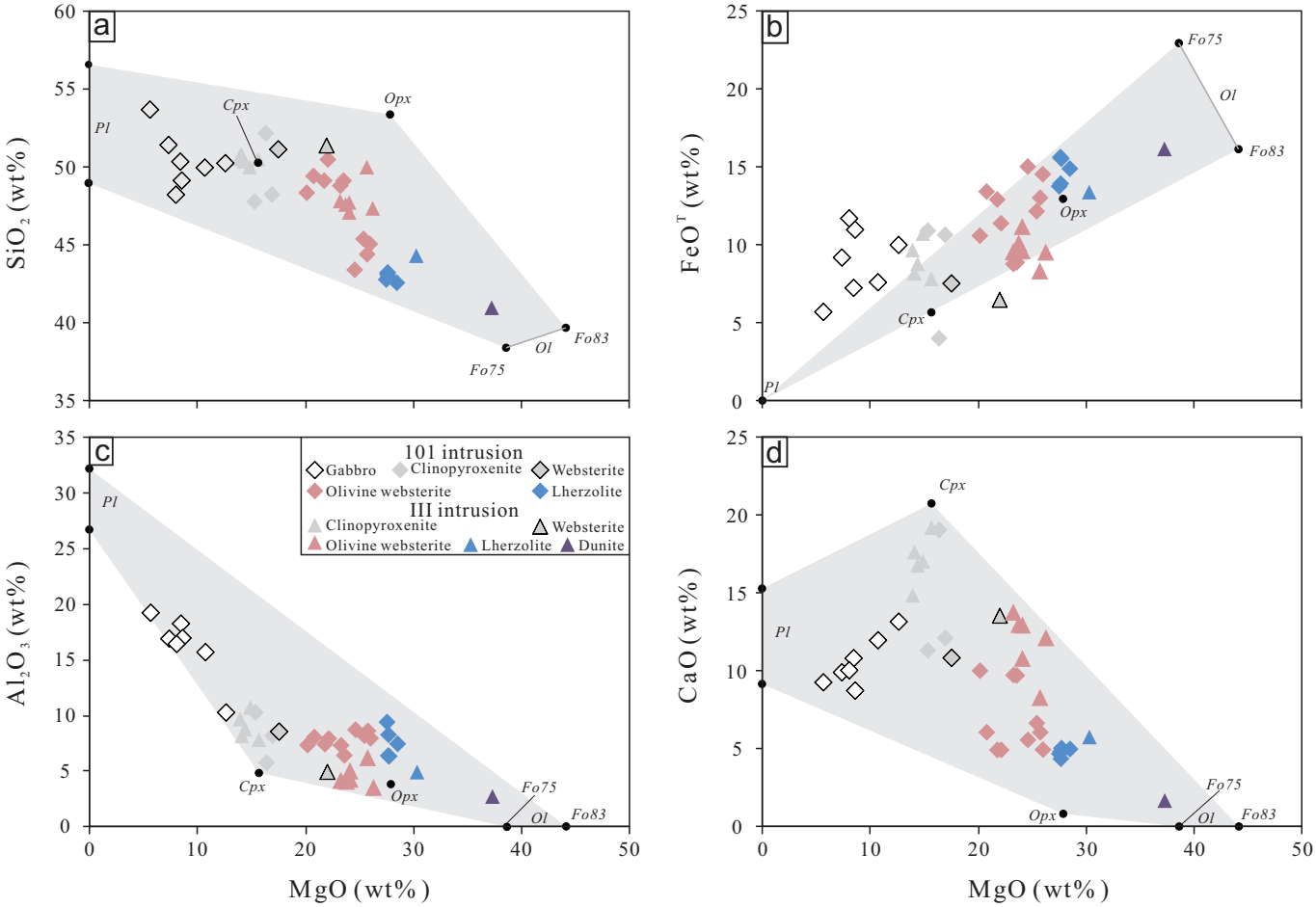

Fig. 5. Variations of whole-rock compositions in the Lengshuiqing intrusions. MgO vs. (a) SiO_2, (b) FeO^T, (c) Al_2O_3, and (d) CaO. Abbreviations: Cpx = clinopyroxene, Ol = olivine, Opx = orthopyroxene, Pl = plagioclase. Data for the Lengshuiqing 101 intrusion are from Zhu et al. (2007).

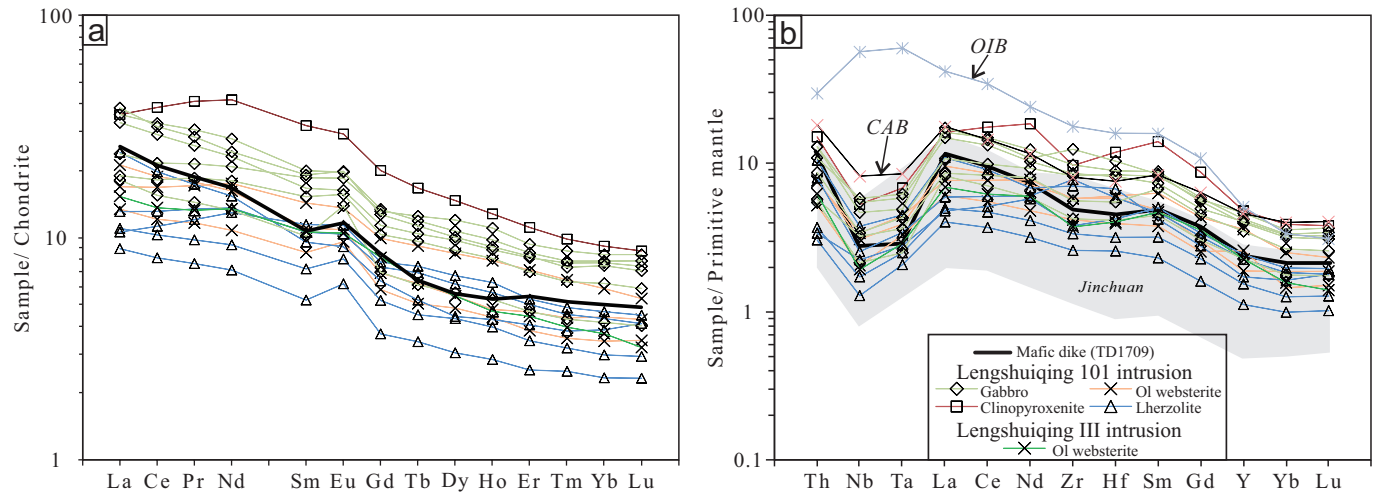

Fig. 6. (a) Chondrite-normalized rare earth element patterns and (b) mantle-normalized immobile trace element patterns of the Lengshuiqing intrusive rocks and an arc-type mafic dike in the region. Data for the Lengshuiqing 101 intrusion are from Zhu et al. (2007). Data for the Jinchuan intrusion are from X. Li et al. (2005), Tonnelier (2010), and Duan et al. (2016). The average values of oceanic island basalts (OIB) and continental arc basalts (CAB) for comparison are from Chusi Li et al. (2015b). The normalizing values for chondrite are from Boynton (1984). The normalizing values for primitive mantle are from Sun and McDonough (1989). Abbreviations: Ol = olivine.

Table 6. Re-Os Isotopes of the Lengshuiqing Magmatic Ni-Cu Ore Deposit

Sample	Intrusion no.	Rock type	Total Re (ppb)	1σ	^{187}Re (ppb)	1σ	^{187}Os (ppb)	1σ	Common Os (ppb)	1σ	^{187}Re/^{187}Os	1σ	^{187}Os/^{187}Os	1σ	$\gamma_{Os}(t)$	(^{187}Os/^{188}Os)
LSZ11	101	Ol websterite	8.26	0.061	5.19	0.038	0.0922	0.0007	0.3517	0.0027	113.4	1.1	2.011	0.003	272	0.451
LSZ11[1]	101	Ol websterite	8.00	0.23	5.03	0.15	0.0919	0.0021	0.3649	0.0127	105.8	4.8	1.935	0.081	295	0.479
LSZ43	101	Clinopyroxenite	19.0	0.14	12.0	0.09	0.1899	0.0014	0.7492	0.0057	122.7	1.2	1.949	0.003	115	0.261
LSZ45	101	Clinopyroxenite	9.36	0.070	5.88	0.044	0.0891	0.0007	0.1472	0.0011	305.8	3.1	4.616	0.007	238	0.410
LSQ1403	III	Clinopyroxenite	1.83	0.014	1.15	0.009	0.0399	0.0003	0.3440	0.0029	24.76	0.26	0.8511	0.002	320	0.511
LSQ1408	III	Ol websterite	5.65	0.042	3.55	0.026	0.0581	0.0004	0.1809	0.0014	148.8	1.5	2.429	0.004	214	0.382
LSQ1411	III	Clinopyroxenite	26.1	0.19	16.4	0.12	0.2594	0.0020	0.5444	0.0041	233.9	2.4	3.681	0.005	282	0.464
GBW04477		Expected[2]	38.6						16.23				0.3363			
		This study	38.8						16.24				0.3360			
		This study	38.0						16.14				0.3369			

Uncertainties of Re-Os isotope compositions are reported for 1σ standard errors; $\gamma_{Os} = 100([^{187}Os/^{188}Os]_{initial}/[^{187}Os/^{188}Os]_{CHUR}-1)$; a present-day (^{187}Os/^{188}Os)now initial = 0.3972, (^{187}Os/^{188}Os)now initial = 0.12757 (Walker and Morgan, 1989), a decay constant $\lambda_{Re} = 1.666 \times 10^{-11}$ year^{-1} (Smoliar et al., 1996) were used in the calculations; the $\gamma_{Os}(t)$ and (^{187}Os/^{188}Os)$_i$ of the Lengshuiqing intrusions were calculated using age of 817 Ma

Abbreviations: Ol = olivine

[1] Duplicate samples

[2] Expected data of the GBW04477 are from http://www.ncrm.org.cn/

with a cumulate origin for the former. The abundances of all REEs are generally higher in the gabbros than in coexisting ultramafic rocks, consistent with a more fractionated parental magma for the gabbro and/or the presence of higher amounts of REE-rich trapped liquid. The mantle-normalized patterns of some immobile incompatible trace elements, including some high field strength elements (HFSE), for the Lengshuiqing intrusions are illustrated in Figure 6b. Pronounced negative Nb-Ta anomalies are present in the Lengshuiqing mafic-ultramafic rocks as well as in a coeval dolerite dike. The dike is fine grained due to rapid cooling, and its bulk composition is presumed to be close to that of the parental liquid. As shown in Figure 6b, these chemical features are common for continental arc basalts and extremely rare for mantle plume-derived magma such as OIBs.

S, Se, and PGE abundances

The sulfide-bearing samples (>0.5 wt % S) from the Lengshuiqing mafic-ultramafic intrusions contain 400 to 2,480 ppm Ni, 40 to 1,390 ppm Cu, 3.0 to 20.3 ppm Se, 4.79 to 45.6 ppb Pd, and 0.02 to 1.99 ppb Ir (Table 3). The listed values for Ni have been corrected for contribution from olivine based on visually estimated abundances of olivine in thin sections and the average Ni contents of the olivine. Strong positive correlations are present between Se and S (Fig. 7a) and between Ni and S (Fig. 7b). Weak positive correlations are present between iridium subgroup PGEs (IPGEs; Ir, Ru, Rh) and S (Fig. 7c-e) and Pd and S (Fig. 7f). No correlation exists between Pt and S.

We have used the method of C. Li et al. (2001) to estimate the abundances of pyrrhotite (Fe_7S_8), pentlandite ($Fe_{4.5}Ni_{4.5}S_8$), and chalcopyrite ($CuFeS_2$) in 100% sulfide and the equation of Barnes and Lightfoot (2005) to calculate the metal tenors in bulk sulfide (i.e., 100% sulfides). The results show good correlations between IPGEs (Ir, Ru, Rh; Fig. 8a, b), no correlation between a palladium subgroup PGE (PPGE; Pt and Pd) and an IPGE such as Ir (Fig. 8c), and no correlation between Ni and Cu (Fig. 8d) in bulk sulfide. The proportions of pyrrhotite, pentlandite, and chalcopyrite for most samples are 75 to 85 wt %, 14 to 17 wt %, and 2 to 7 wt %, respectively. Two other samples (LSQ1403 and LSQ1405) contain 15 to 20 wt % chalcopyrite in 100% sulfide. The mantle-normalized chalcophile element patterns for the bulk sulfide ores (recalculated to 100% sulfides) of the Lengshuiqing deposit, which show depletions of PGEs relative to Ni and Cu plus a negative or positive Pt anomaly in almost every sample from the deposit, are illustrated in Figure 9. The PGE tenors of the Lengshuiqing deposit are significantly lower than those of the Jinchuan deposit.

Sr-Nd-S-Os isotopes

Whole-rock Sr-Nd isotope compositions of the Lengshuiqing mafic-ultramafic intrusions are given in Table 4. The calculated $\varepsilon_{Nd}(t)$ values (t = 817 Ma; Munteanu et al., 2010b) and initial $(^{87}Sr/^{86}Sr)_i$ ratios for these intrusions vary from 1.1 to 5.8 and from 0.7038 to 0.7050, respectively. The $\varepsilon_{Nd}(t)$ values for the Lengshuiqing intrusions are strikingly different from those for the Jinchuan intrusion (Fig. 10). The Jinchuan intrusion is characterized by negative $\varepsilon_{Nd}(t)$ values as low as –12, consistent with a highly enriched source mantle (Duan et al.,

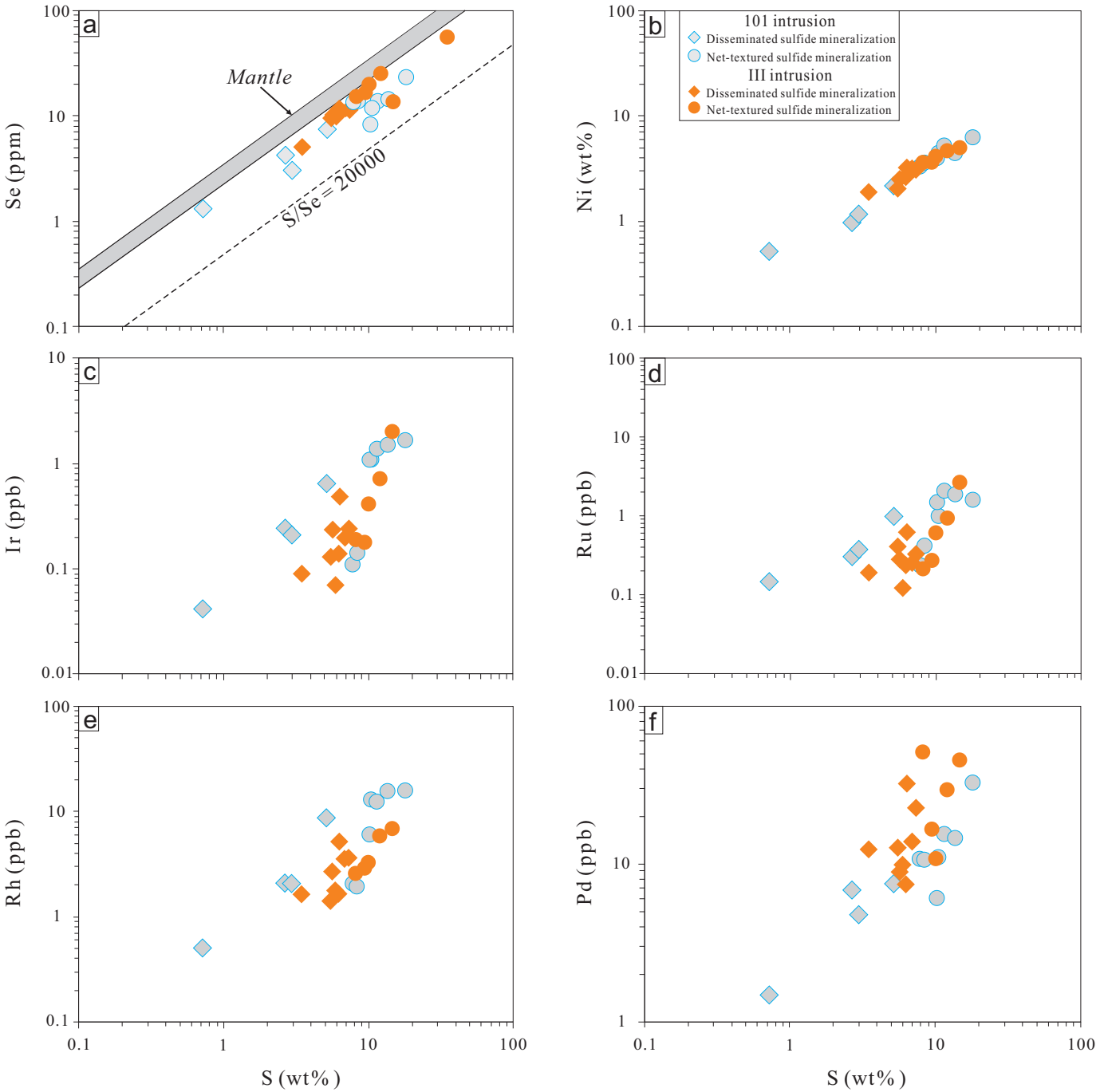

Fig. 7. (a-f) Plots of chalcophile element concentrations vs. S contents in whole rocks from the Lengshuiqing sulfide deposit. Data for mantle are from Eckstrand and Hulbert (1987).

2016). In contrast, the Lengshuiqing intrusions are characterized by positive $\varepsilon_{Nd}(t)$ values as high as 6, consistent with a depleted mantle source. Another important feature is that the Sr-Nd isotope systematics of the Lengshuiqing intrusions and Cenozoic arc basalts are similar (Fig. 10).

Sulfur isotope compositions of the Lengshuiqing Ni-Cu ore deposit are listed in Table 5. One sample has $\delta^{34}S$ = –4.0‰. The remaining samples have $\delta^{34}S$ values varying between –1.0‰ and 1.3‰. These values partially overlap the MORB values of Labidi et al. (2013, 2014), but the range is significantly wider than that defined by the MORB samples (Fig. 11).

Whole-rock Re-Os concentrations and isotope ratios in the Lengshuiqing deposit are given in Table 6. The initial $^{187}Os/^{188}Os$ ratios and $\gamma_{Os}(t)$ values are from 0.261 to 0.510 and from 115 to 320, respectively. Overall, the $\gamma_{Os}(t)$ values for the Lengshuiqing deposit are higher than those for the Jinchuan deposit (Fig. 12a). No correlation between the $\gamma_{Os}(t)$

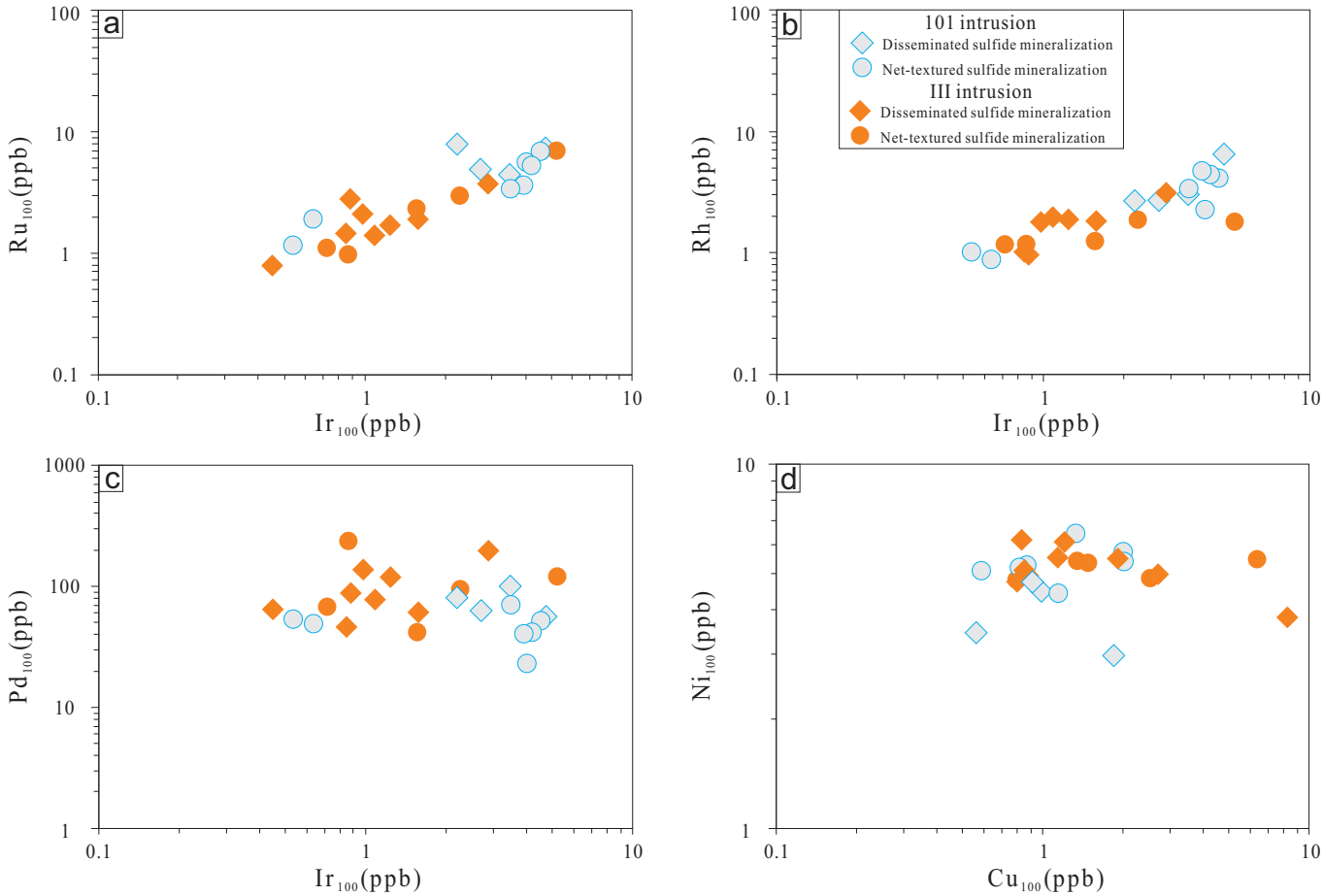

Fig. 8. Correlations between chalcophile elements in recalculated 100% sulfide of mineralized samples from the Lengshuiqing sulfide deposit. (a) Ru_{100} vs. Ir_{100}, (b) Rh_{100} v.s Ir_{100}, (c) Pd_{100} vs. Ir_{100}, and (d) Ni_{100} vs. Cu_{100}.

values and S/Se ratios is observed in the samples from the Lengshuiqing deposit (Fig. 12b).

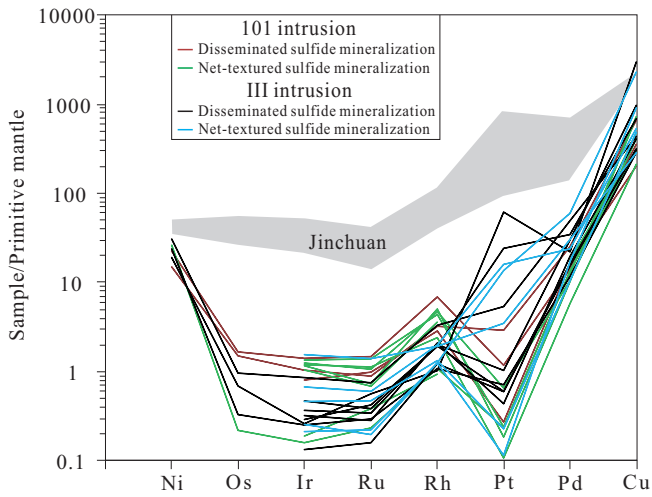

Fig. 9. Mantle-normalized Ni-platinum group element-Cu patterns for the Lengshuiqing sulfide deposit. Data for Jinchuan are taken from C. Li and Ripley (2011). The normalization values are from Barnes and Maier (1999).

Modeling and Discussion

Oxidation state

The Fe-Ni exchange coefficient between olivine and sulfide liquid, or K_D ($[X_{NiS}/X_{FeS}]^{Sulf\text{-}liq}/[X_{NiO}/X_{FeO}]^{Ol}$, molar), is a function of temperature and f_{O_2} (Brenan, 2003). At constant pressure, these two variables together define the oxidation state of a magmatic sulfide system. Barnes et al. (2013) used available experimental data to calibrate the relationship between the K_D and oxidation state of sulfide-bearing magmatic systems. We have used the empirical equation of Barnes et al. (2013) to estimate the oxidation state of the Lengshuiqing magmatic sulfide deposit. The results are illustrated in Figure 13. The estimated oxidation state for the Lengshuiqing deposit is close to QFM + 1 (i.e., f_{O_2} one log unit higher than the value of the quartz-fayalite-magnetite buffer), which is similar to the estimated oxidation states of the two most important magmatic sulfide deposits in China, the rift-related Jinchuan deposit (C. Li and Ripley, 2011) and the arc-type Xiarihamu deposit (Chusi Li et al., 2015a), but is more oxidized than the Voisey's Bay deposit associated with the Nain Anorthosite Suite in Labrador, Canada (C. Li and Naldrett, 1999). The elevated f_{O_2} values alone are insufficient to distinguish processes such as crustal contamination of a plume-derived magma from

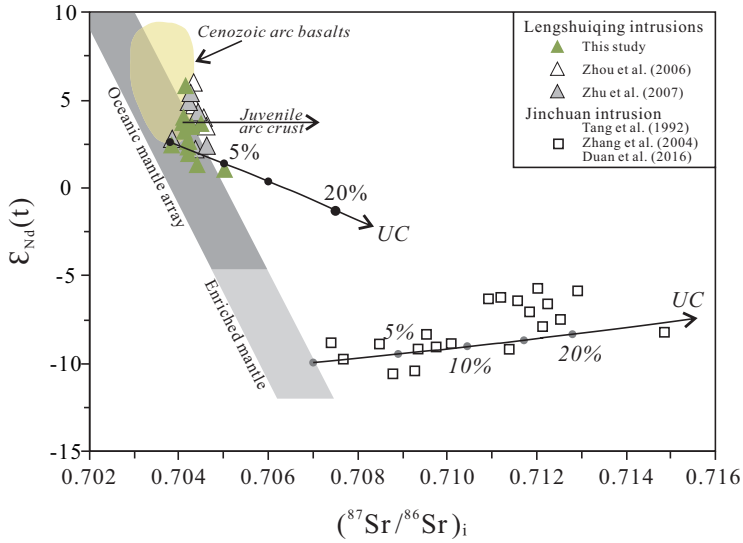

Fig. 10. Plot of whole-rock $\varepsilon_{Nd}(t)$ vs. $(^{87}Sr/^{86}Sr)_i$ for the Lengshuiqing sulfide deposit. The oceanic mantle array is from Zindler and Hart (1986). Values for mixing calculations: mantle-derived melt, 97 ppm Sr, 9.8 ppm Nd, $\varepsilon_{Nd}(t)$ = +2.6, $(^{87}Sr/^{86}Sr)_i$ = 0.7038; UC (Upper crust) (Rudnick and Gao, 2014), 320 ppm Sr, 27 ppm Nd, 10.5 ppm Th, 12 ppm Nb, 31 ppm La, 4.7 ppm Sm, $\varepsilon_{Nd}(t)$ = –7, $(^{87}Sr/^{86}Sr)_i$ = 0.712. The Sr-Nd isotopes of Cenozoic arc basalts worldwide are from a public database (http://www.petdb.org).

derivation of oxidized magma in an arc setting as a result of partial melting of metasomatized asthenospheric mantle, perhaps followed by crustal contamination.

Geochemical and geologic inferences on the origin of plume vs. arc magmatism in the Lengshuiqing region

There are two competing explanations for the observed negative Nb-Ta anomalies in the Lengshuiqing intrusions (Fig. 6): a primary signature of subduction-related magma vs. crustal contamination of mantle plume-derived or continental rift-related magma. As shown in Figure 10, mixing calculations based on Sr-Nd isotope data indicate <5 wt % crustal contamination for the Lengshuiqing intrusions. It is unlikely that such small amounts of crustal contamination can fully account for the large negative Nb-Ta anomalies in the Lengshuiqing intrusions (Fig. 6). The negative Nb-Ta anomalies in the Jinchuan intrusion (Fig. 6) are more consistent with crustal contamination of rift-related magma, because the degrees of crustal contamination inferred from the Sr-Nd isotope data are much higher, up to 30% (Fig. 10). Thus, we favor the interpretation that the Lengshuiqing intrusions are derived from arc basalts. Such a view is also supported by the chemical compositions of rock-forming minerals such as olivine, Cr spinel, and clinopyroxene in the intrusions (Fig. 4). In addition, the association of the contemporary Tongde diorite batholith and the large age span of Neoproterozoic basaltic magmatism from ~860 to ~740 Ma in the region are consistent with an arc model rather than the mantle plume model. Finally, recent seismic data from the SINOPROBE project also support the interpretation that the western rim of the Yangtze craton was a subduction zone in the Neoproterozoic (Gao et al., 2016).

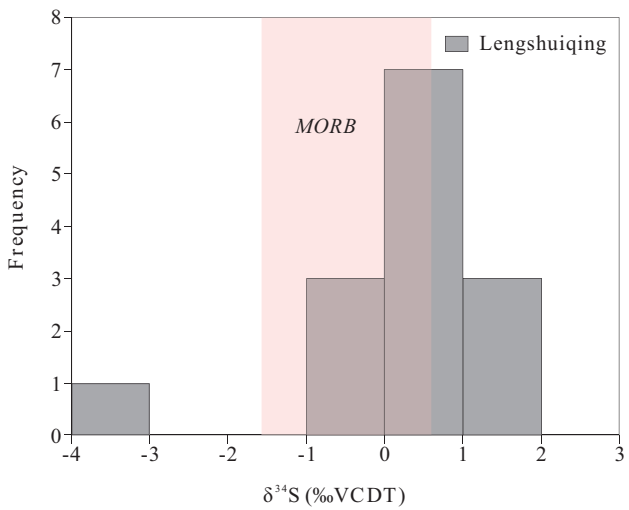

Fig. 11. Histogram of $\delta^{34}S$ values of sulfides from the Lengshuiqing sulfide deposit. The range of $\delta^{34}S$ for mid-ocean ridge basalts (MORB) is –1.57 to 0.60‰, from Labidi et al. (2013, 2014). VCDT = Vienna-Canyon Diablo troilite.

Controls on PGE tenors

Strong positive correlation between Ni and S in the Lengshuiqing deposit (Fig. 7b), which is consistent with similar proportions of pentlandite in the bulk sulfide, indicates that the Ni tenors of bulk sulfide ores are mainly controlled by magmatic sulfide liquids with similar Ni compositions. A weaker correlation between Cu and S can be explained by sulfide mineral fractionation at the sample scale. The lack of correlation between Pt and S is consistent with the presence of both positive and negative Pt anomalies in the samples (Fig. 9). Weak correlations between other PGEs and S (Fig. 7c-f) and good correlations between IPGEs (Fig. 8a, b) reflect variable PGE compositions in the bulk sulfide ores. The main controls on such variations, as summarized in Naldrett (2011), are (1)

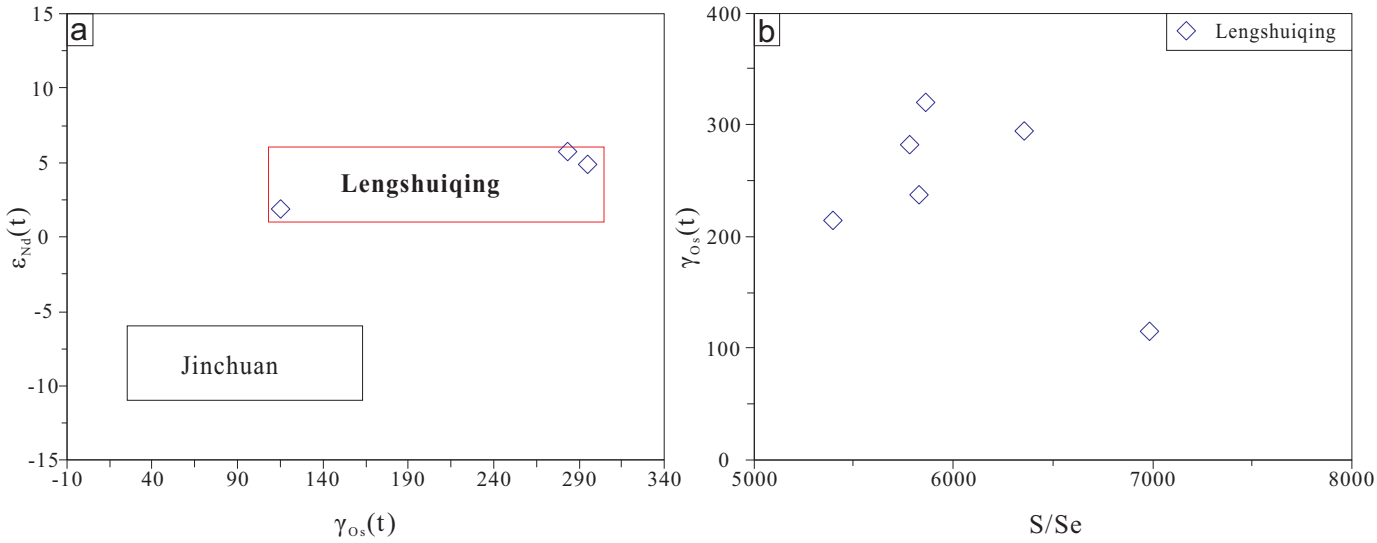

Fig. 12. Plots of (a) $\varepsilon_{Nd}(t)$ vs. $\gamma_{Os}(t)$ and (b) $\gamma_{Os}(t)$ vs. S/Se values for the Lengshuiqing sulfide deposit. Nd and Os isotope data for Jinchuan intrusion are from Zhang et al. (2004), X. Li et al. (2005), and Yang et al. (2005, 2008).

variable initial PGE contents in magma, (2) variable R factors (magma/sulfide mass ratios), and (3) fractional crystallization of monosulfide solid solution (MSS) from sulfide liquid. Commonly the last process has greater effect on the chalcophile element compositions of semimassive and massive sulfide ores than on compositions of disseminated and net-textured sulfide ores (Naldrett et al., 1994). Since our main concerns for the Lengshuiqing deposit are the first two variables, in the following we will focus on the disseminated and net-textured sulfide ores of the deposit. Initial magma PGE contents and R factors can be estimated using the equation of Campbell and Naldrett (1979). Due to their extremely high partition coefficients (D values) between sulfide liquid and magma, the concentrations of PGEs in a sulfide liquid depend on both R factors and their initial contents in magma. Hence, it

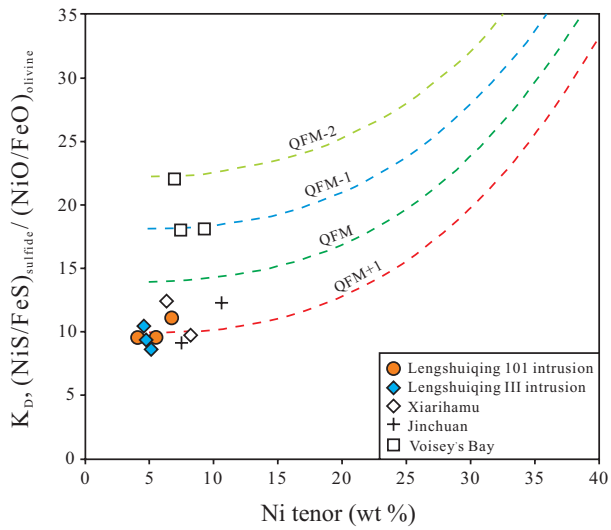

Fig. 13. The oxidation state of the Lengshuiqing sulfide deposit determined using olivine compositions and Ni contents in bulk sulfide. The base of the plot and the data for Jinchuan and Voisey's Bay deposits are from Barnes et al. (2013). Data for Xiarihamu are from Chusi Li et al. (2015a).

is important to first estimate the R factors using other chalcophile elements that have significantly lower D values such as Ni or Cu. Due to the effect of olivine fractional crystallization, the contents of Ni in magma are more variable than Cu. Thus, we use Cu in our calculation. Using an experimental D_{Cu} value of 1,000 for the basaltic system (Ripley et al., 2002; Mungall and Brenan, 2014) and an initial Cu content of 100 ppm, the upper limit for primitive arc basalts (Lee et al., 2012), we have obtained an R factor of ~150 for a disseminated sulfide ore sample with the lowest Cu tenor (~1 wt %) in the Lengshuiqing deposit. This value is used as the lower limit for the deposit. Using Pd and Ir to represent PPGEs and IPGEs, respectively, and the recommended D values of 10^5 for these elements (Mungall and Brenan, 2014), the initial concentrations of Pd and Ir in the Lengshuiqing magma are estimated to have been 0.25 and 0.006 ppb, respectively (Fig. 14). The effects of MSS fractional crystallization shown in the figure are estimated using the MSS/liquid D values from C. Li et al. (1996). The Lengshuiqing samples all plot within the field composed of sulfide fractionated liquid and MSS. The estimated initial contents of Pd and Ir in the Lengshuiqing magma are about two orders of magnitude lower than the average values for PGE undepleted picrites of continental flood basalt provinces such as Emeishan (C. Li et al., 2016) and Siberia (Lightfoot and Keays, 2005) but similar to the results for two major subduction-related magmatic sulfide deposits in China: the Heishan (Xie et al., 2014) and Xiarihamu (Zhang et al., 2017) deposits. Therefore, other than the weak influence of postmagmatic hydrothermal alteration and/or nugget effects (especially for Pt), the PGE tenor variations of the Lengshuiqing deposit can be explained by variable R factors, and the weak correlations between PGEs and S can be attributed variable amounts of MSS and coexisting sulfide liquid in the assemblages.

Causes of sulfide saturation

The addition of crustal sulfur into mantle-derived magmas is widely known to be the most effective process for the

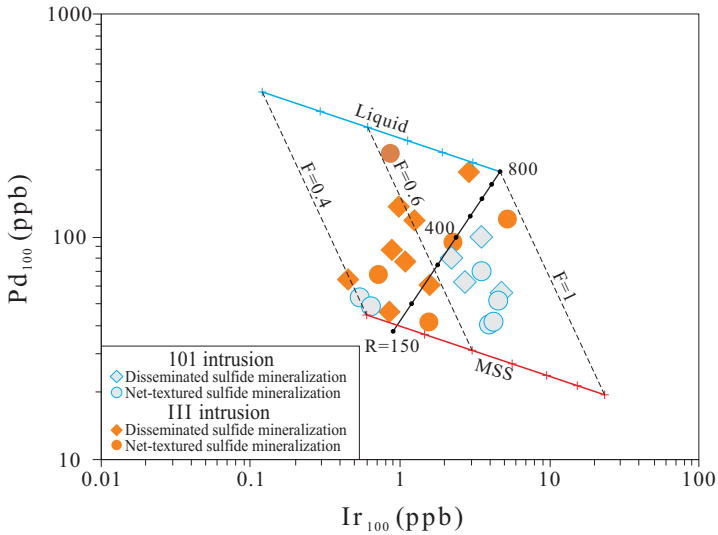

Fig. 14. Plot of Pd vs. Ir in recalculated 100% sulfide of mineralized samples from the Lengshuiqing sulfide deposit, compared with model trends. Line marked with "R" represents sulfide liquids segregated from magma with variable R factors (magma/sulfide mass ratio). The numbers beside the line are the R factors. Numbered F is the fraction of remaining sulfide liquid. The sulfide/magma partition coefficients for Pd and Ir are assumed to be 10^5. The monosulfide solid solution (MSS)/liquid partition coefficients for Ir and Pd are assumed to be 5 and 0.1, respectively. The concentrations of 0.25 ppb Pd and 0.006 ppb Ir for the Lengshuiqing intrusions can reproduce the overall trends of the samples. Displacements from these trends can be explained by sulfide liquid fractionation.

formation of magmatic sulfide ore deposits (e.g., Ripley and Li, 2003; Robertson et al., 2015; Ripley et al., 2017). The wider range of $\delta^{34}S$ values compared to the range of MORB values for the Lengshuiqing deposit (Fig. 11) is consistent with the involvement of crustal sulfur in the genesis of the Lengshuiqing deposit. This is also supported by S/Se ratios for the Lengshuiqing deposit (Fig. 7a), which are displaced from mantle ratios (2,850–4,350; Eckstrand and Hulbert, 1987) toward those of the crust (>20,000: Eckstrand et al., 1989). Another line of evidence that supports the importance of crustal contamination in the genesis of the Lengshuiqing deposit is the elevated $\gamma_{Os}(t)$ values (Fig. 12). In crustal environments Os is commonly associated with sulfides or organic matter. Because Sr and Nd, which are lithophile elements that typically occur in silicate minerals rather than sulfides, do not show isotopic evidence for significant crustal contamination (Fig. 10), selective contamination involving sulfide minerals and/or organic matter in country rocks is indicated.

The forsterite contents of olivine in the Lengshuiqing deposit are 75 to 86 mol %. The higher end is 4 mol % lower than expected for olivine crystallizing from a primitive mantle-derived magma such as the parental magma for the arc-type Xiarihahu magmatic sulfide deposit (Chusi Li et al., 2015a). The results of MELTS simulation by these authors indicate that the most primitive olivine compositions from the Lengshuiqing deposit represent ~13% fractional crystallization of olivine alone from a magma derived from primitive asthenospheric mantle in an arc setting. At 30 kb (~90 km depth), the content of S in a primitive arc magma in equilibrium with olivine of Fo_{90}, consistent with derivation from the parental magma for the Xiarihamu deposit (Chusi Li et al., 2015a), is estimated to be ~1,500 ppm using the equation of C. Li and Ripley (2009). After 13% fractional crystallization, the content of S in the fractionated liquid will increase to 1,724 ppm. At 2 kb (~6 km depth), the S content at sulfide saturation in the fractionated magma is estimated to be ~2,000 ppm using the equation of C. Li and Ripley (2009), which is 276 ppm higher than the actual content of S in the magma. The modeling results indicate that sulfide saturation in the Lengshuiqing magma was not triggered by fractional crystallization alone. Other factors such as selective assimilation of crustal sulfides also played an important role.

Genetic model and exploration implications

Regional geologic constraints summarized by previous researchers and the petrological and geochemical evidences from this study strongly support the view that the Lengshuiqing magmatic sulfide deposit is related to arc basaltic magmatism (Fig. 15a). The inferred different tectonic settings for the Lengshuiqing (subduction-related) and Jinchuan (rift-related) magmatic sulfide deposits help to explain many different mineralogic and geochemical features of these two deposits that have similar ages but occur in different Precambrian continental blocks in China (Fig. 1a).

The recognition of the Lengshuiqing magmatic sulfide deposit as an arc-type deposit bears some significant implications for Ni exploration. The fact that sulfide saturation took place during or prior to the crystallization of host silicate minerals, together with the fact that sulfide and olivine accumulated together in such small bodies (Fig. 2b, c), lead us to propose an open ore-forming system for each of the mineralized mafic-ultramafic intrusions in the Lengshuiqing area. We envision that the magma was charged with olivine and small immiscible sulfide liquid droplets upon arrival. Most of the olivine and sulfide droplets settled down to form sulfide-olivine crystal mushes, and much of the transporting magma continued to ascend to the higher levels (Fig. 15b).

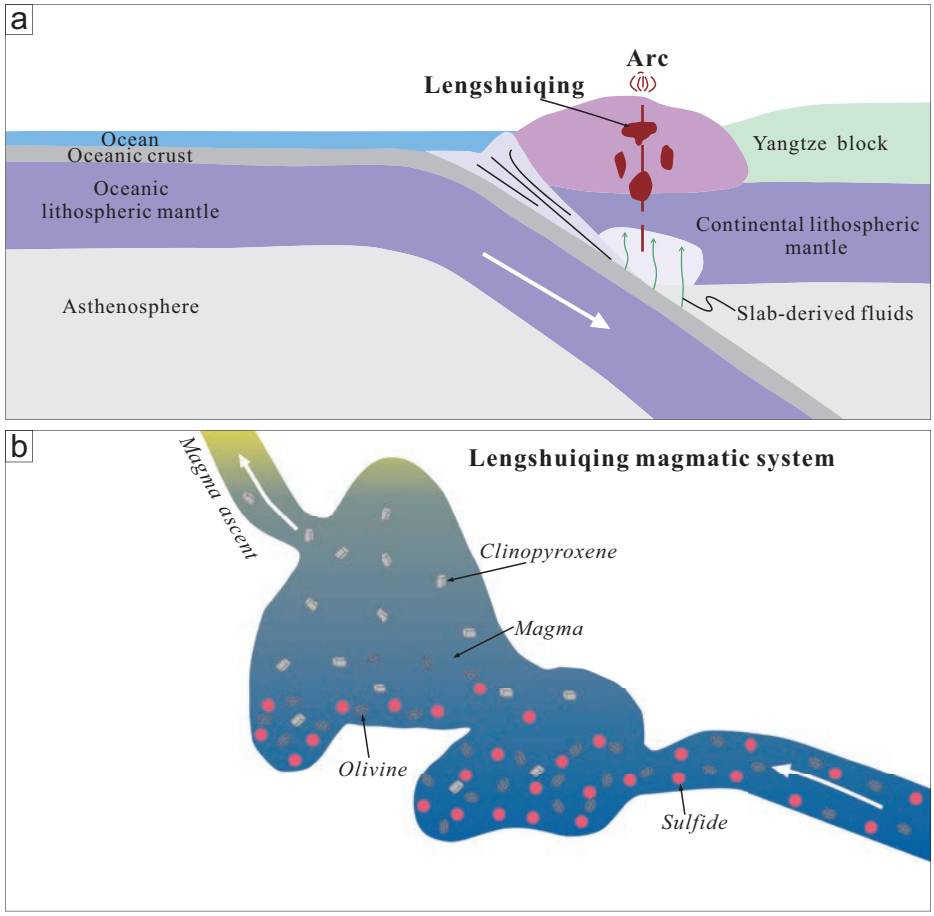

Fig. 15. Conceptual genetic models for the Lengshuiqing magmatic sulfide deposit, (a) showing that the host intrusions are the mafic-ultramafic intrusions formed from subduction-related mafic magma and (b) showing that the sulfide droplets and olivine crystals carried by the ascending magma settled down to the base of the intrusions to form the orebodies.

Globally, the Lengshuiqing deposit provides another good example for Ni exploration in Paleozoic and Precambrian orogenic belts that have undergone significant uplift and erosion. Arc basaltic magmatism is commonly very protracted, so at the regional scale the exploration targets are not limited to the mafic-ultramafic intrusions that are truly coeval with the Lengshuiqing sulfide ore-bearing intrusions. As shown in Figure 2a, there are numerous Neoproterozoic mafic-ultramafic intrusions, including the Lengshuiqing sulfide ore-bearing intrusions, in the Yanbian region in the western margin of the Yangtze craton. The ages and sizes of these Neoproterozoic mafic-ultramafic intrusions may vary significantly, but they should all be evaluated for the potential of hosting arc-type magmatic sulfide deposits.

Conclusions

The most important findings from this study are given below:

1. The host intrusions of the Neoproterozoic Lengshuiqing magmatic Ni-Cu ore deposits in the western margin of the Yangtze craton, such as the 101 and III mafic-ultramafic intrusions, resemble arc cumulates based on similarities in mineral compositions and trace element geochemistry.
2. Olivine chemistry indicates that the parental magma for the Lengshuiqing ultramafic rocks was a moderately fractionated basaltic magma.
3. S/Se and Sr-Nd-Os-S isotopes reveal that crustal contamination of the magma was selective instead of wholesale.
4. Both fractional crystallization and addition of crustal sulfur may have played an important role in triggering sulfide saturation in the Lengshuiqing magma.
5. Other subduction-related mafic-ultramafic intrusions of Neoproterozoic ages in the Yanbian region in the western margin of the Yangtze craton are good exploration targets for Lengshuiqing-type magmatic Ni-Cu deposits.

Acknowledgments

This study was supported by the Strategic Priority Research Program of the Chinese Academy of Sciences (grant XDB18030204) and the National Science Foundation of China (grants 41425011, 41572074, and 41273049). We thank M.W. Liu for assistance in mineral chemical analysis and G.P. Bao, Y. Huang, J. Hu, L. Qi, W.J. Qu, and J. Wang for their advice and guidance in whole-rock chemical and isotopic analysis. Constructive reviews from the reviewers and editorial advice from the editors are greatly appreciated.

REFERENCES

Bai, Z.J., Zhong, H., Naldrett, A.J., Zhu, W.G., and Xu, G.W., 2012, Whole-rock and mineral composition constraints on the genesis of the giant Hongge Fe-Ti-V oxide deposit in the Emeishan large igneous province, southwest China: Economic Geology, v. 107, p. 507–524.

Barnes, S.J., and Kunilov, V.Y., 2000, Spinels and Mg ilmenites from the Noril'sk 1 and Talnakh intrusions and other mafic rocks of the Siberian flood basalt province: Economic Geology, v. 95, p. 1701–1717.

Barnes, S.J., and Tang, Z.L., 1999, Chrome spinels from the Jinchuan Ni-Cu sulfide deposit, Gansu province, People's Republic of China: Economic Geology, v. 94, p. 343–356.

Barnes, S.J., Godel, B., Gürer, D., Brenan, J.M., Robertson, J., and Paterson, D., 2013, Sulfide-olivine Fe-Ni exchange and the origin of anomalously Ni rich magmatic sulfides: Economic Geology, v. 108, p. 1971–1982.

Barnes, S.-J., and Lightfoot, P.C., 2005, Formation of magmatic nickel sulfide ore deposits and processes affecting their copper and platinum-group contents: Economic Geology 100th Anniversary Volume, p. 179–213.

Barnes, S.-J., and Maier, W.D., 1999, The fractionation of Ni, Cu, and the noble metals in silicate and sulfide liquids: Dynamic processes in magmatic ore deposits and their application to mineral exploration: Geological Association of Canada Short Course Notes, v. 13, p. 69–106.

Boynton, W.V., 1984, Geochemistry of the rare earth elements: Meteorite studies, *in* Henderson, P., ed., Rare earth element geochemistry: Amsterdam, Elsevier, p. 63–114.

Brenan, J.M., 2003, Effects of f_{O_2}, f_{S_2}, temperature, and melt composition on Fe-Ni exchange between olivine and sulfide liquid: Implications for natural olivine-sulfide assemblages: Geochimica et Cosmochimica Acta, v. 67, p. 2663–2681.

Campbell, I., and Naldrett, A.J., 1979, The influence of silicate:sulfide ratios on the geochemistry of magmatic sulfides: Economic Geology, v. 74, p. 1503–1506.

Chen, L.M., Song, X.Y., Danyushevsky, L.V., Xiao, J.F., Li, S.B., and Guan, J.X., 2009, Correlation between Ni and MgO contents of olivine in segment I of the Jinchuan intrusion, NW China, and its geological implication: Acta Petrologica Sinica, v. 25, p. 3369–3378 (in Chinese with English abstract).

Du, A.D., Wu, S.Q., Sun, D.Z., Wang, S.X., Qu, W.J., Markey, R., Stain, H., Morgan, J., and Malinovskiy, D., 2004, Preparation and certification of Re-Os dating reference materials: Molybdenites HLP and JDC: Geostandards and Geoanalytical Research, v. 28, p. 41–52.

Du, L.L., Guo, J.H., Nutman, A.P., Wyman, D., Geng, Y.S., Yang, C.G., Liu, F.L., Ren, L.D., and Zhou, X., 2014, Implications for Rodinia reconstructions for the initiation of Neoproterozoic subduction at ~860 Ma on the western margin of the Yangtze block: Evidence from the Guandaoshan pluton: Lithos, v. 196, p. 67–82.

Duan, J., Li, C., Qian, Z., Jiao, J., Ripley, E.M., and Feng, Y., 2016, Multiple S isotopes, zircon Hf isotopes, whole-rock Sr-Nd isotopes, and spatial variations of PGE tenors in the Jinchuan Ni-Cu-PGE deposit, NW China: Mineralium Deposita, v. 51, p. 557–574.

Eckstrand, O.R., and Hulbert, L.J., 1987, Selenium and the source of sulfur in magmatic nickel and platinum deposits: Geological Association of Canada-Mineralogical Association Canada Program with Abstracts, v. 12, p. 40.

Eckstrand, O.R., Grinenko, L.N., Krouse, H.R., Paktunc, A.D., Schwann, P.L., and Scoates, R.F.J., 1989, Preliminary data on sulphur isotopes and Se/S ratios, and the source of sulphur in magmatic sulphides from the Fox River sill, Molson dykes and Thompson nickel deposits, northern Manitoba: Geological Survey of Canada, Current Research Part C, Paper 89–1C, p. 235–242.

Gao, R., Chen, C., Wang, H.Y., and Lu, Z.W., 2016, SINOPROBE deep reflection profile reveals a Neoproterozoic subduction zone beneath Sichuan basin: Earth and Planetary Science Letters, v. 454, p. 86–91.

Greentree, M.R., and Li, Z.X., 2008, The oldest known rocks in southwestern China: SHRIMP U-Pb magmatic crystallization age and detrital provenance analysis of the Paleoproterozoic Dahongshan Group: Journal of Asian Earth Sciences, v. 33, p. 289–302.

Greentree, M.R., Li, Z.X., Li, X.H., and Wu, H., 2006, Latest Mesoproterozoic to earliest Neoproterozoic basin record of the Sibao orogenesis in western South China and relationship to the assembly of Rodinia: Precambrian Research, v. 151, p. 79–100.

Han, C.M., Xiao, W.J., Su, B.X., Sakyi, P.A., Ao, S.J., Zhang, J., Wan, B., Song, D.F., and Wang, Z.M., 2016, Ages and tectonic implications of the mafic-ultramafic-carbonatite intrusive rocks and associated Cu-Ni, Fe-P, and apatite-vermiculite deposits from the Quruqtagh district, NW China: Ore Geology Reviews, doi: 10.1016/j.oregeorev.2016.07.011.

Kamenetsky, V.S., Crawford, A.J., and Meffre, S., 2001, Factors controlling chemistry of magmatic spinel: An empirical study of associated olivine, Cr spinel, and melt inclusions from primitive rocks: Journal of Petrology, v. 42, p. 655–671.

Kamenetsky, V.S., Elburg, M., Arculus, R., and Thomas, R., 2006, Magmatic origin of low-Ca olivine in subduction-related magmas: Coexistence of contrasting magmas: Chemical Geology, v. 233, p. 346–357.

Labidi, J., Cartigny, P., and Moreira, M., 2013, Nonchondritic sulphur isotope composition of the terrestrial mantle: Nature, v. 501, p. 208–211.

Labidi, J., Cartigny, P., Hamelin, C., Moreira, M., and Dosso, L., 2014, Sulfur isotope budget (^{32}S, ^{33}S, ^{34}S, and ^{36}S) in Pacific-Antarctic ridge basalts: A record of mantle source heterogeneity and hydrothermal sulfide assimilation: Geochimica et Cosmochimica Acta, v. 133, p. 47–67.

Le Bas, M.J., 1962, The role of aluminum in igneous clinopyroxenes with relation to their parentage: American Journal of Science, v. 260, p. 267–288.

Lee, C.T., Luffi, P., Chin, E.J., Bouchet, R., Dasgupta, R., Morton, D.M., Le Roux V., Yin, Q.Z., and Jin D., 2012, Copper systematics in arc magmas and implications for crust-mantle differentiation: Science, v. 336, p. 64–68.

Li, Chao, Yang, X., Zhao, H., Zhou, L.M., Du, A.D., Li, X.W., Qu, W.J., 2015, High precise isotopic measurements of pg-ng Os by negative ion thermal ionization mass spectrometry: Rock and Mineral Analysis, v. 34, p. 392–398 (in Chinese with English abstract).

Li, Chusi, and Naldrett, A.J., 1999, Geology and petrology of the Voisey's Bay intrusion: Reaction of olivine with sulfide and silicate liquids: Lithos, v. 47, p. 1–31.

Li, C., and Ripley, E.M., 2009, Sulfur contents at sulfide-liquid or anhydrite saturation in silicate melts: Empirical equations and example applications: Economic Geology, v. 104, p. 405–412.

——2011, The giant Jinchuan Ni-Cu-(PGE) deposit: Tectonic setting, magma evolution, ore genesis, and exploration implications: Reviews in Economic Geology, v. 17, p. 163–180.

Li, C., Barnes, S.-J., Makovicky, E., Rose-Hansen, J., and Makovicky, M., 1996, Partitioning of nickel, copper, iridium, rhenium, platinum, and palladium between monosulfide solid solution and sulfide liquid: Effects of composition and temperature: Geochimica et Cosmochimica Acta, v. 60, p. 1231–1238.

Li, C., Maier, W.D., and De Waal, S.A., 2001, Magmatic Ni-Cu versus PGE deposits: Contrasting genetic controls and exploration implications: South African Journal of Geology, v. 104, p. 309–318.

Li, C., Xu, Z., De Waal, S.A., Ripley, E.M., and Maier, W.D., 2004, Compositional variations of olivine from the Jinchuan Ni-Cu sulfide deposit, western China: implications for ore genesis: Mineralium Deposita, v. 39, p. 159–172.

Li, C., Naldrett, A.J., and Ripley, E.M., 2007, Controls on the Fo and Ni contents of olivine in sulfide-bearing mafic/ultramafic intrusions: Principles, modeling, and examples from Voisey's Bay: Earth Science Frontiers, v. 14, p. 177–183.

Li, C., Thakurta, J., and Ripley, E.M., 2012, Low-Ca contents and kink-banded textures are not unique to mantle olivine: Evidence from the Duke Island Complex, Alaska: Mineralogy and Petrology, v. 104, p. 147–153.

Li, C., Zhang, Z., Li, W., Wang, Y., Sun, T., and Ripley, E.M., 2015a, Geochronology, petrology, and Hf-S isotope geochemistry of the newly discovered Xiarihamu magmatic Ni-Cu sulfide deposit in the Qinghai-Tibet plateau, western China: Lithos, v. 216–217, p. 224–240.

Li, C., Arndt, N.T., Tang, Q., and Ripley, E.M., 2015b, Trace element indiscrimination diagrams: Lithos, v. 232, p. 76–83.

Li, C., Ripley, E.M., Tao, Y., and Hu, R., 2016, The significance of PGE variations with Sr-Nd isotopes and lithophile elements in the Emeishan flood basalt province from SW China to northern Vietnam: Lithos, v. 248–251, p. 1–11.

Li, X.H., Li, Z.X., Zhou, H.W., Liu, Y., Liang, and X.R., 2002, U-Pb zircon geochronological, geochemical, and Nd isotopic study of Neoproterozoic basaltic magmatism in western Sichuan: Petrogenesis and geodynamic implications: Earth Science Frontiers, v. 9, p. 329–338 (in Chinese with English abstract).

Li, X.H., Su, L., Chung, S.L., Li, Z.X., Liu, Y., Song, B., and Liu, D.Y., 2005, Formation of the Jinchuan ultramafic intrusion and the world's third largest Ni-Cu sulfide deposit: Associated with the ~825 Ma south China mantle plume?: Geochemistry, Geophysics, Geosystems, v. 6, p. 1–16.

Li, X.H., Li, Z.X., Sinclair, J.A., Li, W.X., and Carter, G., 2006, Revisiting the "Yanbian Terrane": Implications for Neoproterozoic tectonic evolution of the western Yangtze block, South China: Precambrian Research, v. 151, p. 14–30.

Li, Z.X., Li, X.H., Kinny, P.D., and Wang, J., 1999, The breakup of Rodinia: Did it start with a mantle plume beneath South China?: Earth and Planetary Science Letters, v. 173, p. 171–181.

Li, Z.X., Li, X., Kinny, P.D., Wang, J., Zhang, S., and Zhou, H., 2003, Geochronology of Neoproterozoic synrift magmatism in the Yangtze craton, South China, and correlations with other continents: Evidence for a mantle superplume that broke up Rodinia: Precambrian Research, v. 122, p. 85–109.

Lightfoot, P.C., and Keays, R.R., 2005, Siderophile and chalcophile metal variations in flood basalts from the Siberian trap, Noril'sk region: Implications for the origin of the Ni-Cu-PGE sulfide ores: Economic Geology, v. 100, p. 439–462.

Loucks, R.R., 1990, Discrimination of ophiolitic from nonophiolitic ultramafic-mafic allochthons in orogenic belts by the Al/Ti ratio in clinopyroxene: Geology, v. 18, p. 346–349.

Lugmair, G.W., and Harti, K., 1978, Lunar initial $^{143}Nd/^{144}Nd$: Differential evolution of the lunar crust and mantle: Earth and Planetary Science Letters, v. 39, p. 349–357.

Mungall, J.E., and Brenan, J.M., 2014, Partitioning of platinum group elements and Au between sulfide liquid and basalt and the origins of mantle-crust fractionation of the chalcophile elements: Geochimica et Cosmochimica Acta, v. 125, p. 265–289.

Munteanu, M., Wilson, A.H., Yao, Y., Jiang, S.Y., Chunnett, G., Luo, Y.N., Mafurutu, L., and Phadgi, R., 2010a, A conduit-related genesis of the Lengshuiqing intrusive assemblage (Sichuan, SW China): Journal of Volcanology and Geothermal Research, v. 189, p. 118–130.

Munteanu, M., Wilson, A.H., Yao, Y., Chunnett, G., and Luo, Y., 2010b, Sequence of magma emplacement and sulfide saturation in the Gaojiacun-Lengshuiqing intrusive complex (SW China): Mineralium Deposita, v. 45, p. 517–529.

Munteanu, M., Wilson, A., Yao, Y., Harris, C., Chunnett, G., and Luo, Y., 2010c, The Tongde dioritic pluton (Sichuan, SW China) and its geotectonic setting: Regional implications of a local-scale study: Gondwana Research, v. 18, p. 455–465.

Munteanu, M., Wilson, A.H., Yao, Y., Chunnett, G., Luo, Y., and Sibanda, S., 2011, The Lengshuiqing Ni-Cu deposit, Sichuan, southwestern China: Ore characteistics and genesis: Canadian Mineralogist, v. 49, p. 1599–1626.

Munteanu, M., Wilson, A.H., Costin, G., Yao, Y., Lum, J. E., Jiang, S.Y., Jourdan, F., Chunnett, G., and Cioacă, M.E., 2017, The Mafic-ultramafic dykes in the Yanbian terrane (Sichuan Province, SW China): Record of magma differentiation and emplacement in the Emeishan large igneous province: Journal of Petrology, v. 58, p. 513–538.

Naldrett, A.J., 2011, Fundamentals of magmatic sulfide deposits: Reviews in Economic Geology, v. 17, p. 1–50.

Naldrett, A.J., Asif, M., Gorbachev, N.S., Kunilov, V.E., Stehkin, A.I., Fedorenko, V.A., and Lightfoot, P.C., 1994, The composition of the Ni-Cu ores of the Noril'sk region: Proceedings of the Sudbury Noril'sk Symposium: Ontario Geological Survey, Special Publication, v. 5, p. 357–372.

Nier, A.O., 1938, The isotopic constitution of strontium, barium, bismuth, thallium, and mercury: Physical Review, v. 54, p. 275.

Niu, J., Li, Z.X., and Zhu, W.G., 2015, Palaeomagnetism and geochronology of mid-Neoproterozoic Yanbian dykes, South China: Implications for a c. 820–800 Ma true polar wander event and the reconstruction of Rodinia: Geological Society, London, Special Publications, v. 424, p. 191–211.

Qi, L., Jing, H., and Gregoire, D.C., 2000, Determination of trace elements in granites by inductively coupled plasma mass spectrometry: Talanta, v. 51, p. 507–513.

Qi, L., Gao, J., Huang, X., Hu, J., Zhou, M.F., and Zhong, H., 2011, An improved digestion technique for determination of platinum group elements in geological samples: Journal of Analytical Atomic Spectrometry, v. 26, p. 1900–1904.

Ripley, E.M., and Li, C., 2003, Sulfur isotope exchange and metal enrichment in the formation of magmatic Cu-Ni-(PGE) deposits: Economic Geology, v. 98, p. 635–641.

Ripley, E.M., Brophy, J.G., and Li, C., 2002, Copper solubility in a basaltic melt and sulfide liquid/silicate melt partition coefficients of Cu and Fe: Geochimica et Cosmochimica Acta, v. 66, p. 2791–2800.

Ripley, E.M., Wernette, B.W., Ayre, A., Li, C., Smith, J.M., Underwood, B.S., and Keays, R.R., 2017, Multiple S isotope studies of the Stillwater Complex and country rocks: An assessment of the role of crustal S in the origin of PGE enrichment found in the JM Reef and related rocks: Geochimica et Cosmochimica Acta, v. 214, p. 226–245.

Robertson, J., Ripley, E.M., Barnes, S.J., and Li, C., 2015, Sulfur liberation from country rocks and incorporation in mafic magmas: Economic Geology, v. 110, p. 1111–1123.

Rudnick, R.L., and Gao, S., 2014, Composition of the continental crust, *in* Rudnick, R.L., ed., Treatise on geochemistry: Amsterdam, Elsevier, p. 1–51.

Scheel, J.E., Scoates, J.S., and Nixon, G.T., 2009, Chromian spinel in the Turnagain Alaskan-type ultramafic intrusion, northern British Columbia, Canada: Canadian Mineralogist, v. 47, p. 63–80.

Smoliar, M.I., Walker, R.J. and Morgan, J.W., 1996, Re-Os ages of group IIA, IIIA, IVA, and VIB iron meteorites: Science, v. 271, p. 1099–1102.

Steiger, R.H., and Jager, E., 1977, Subcommission on geochronology: Convention on the use of decay constants in geo- and cosmochronology: Earth and Planetary Science Letters, v. 36, p. 359–362.

Studley, S., Ripley, E., Elswick, E., Dorais, M., Fong, J., and Finkelstein, D., 2002, Analysis of sulfides in whole-rock matrices by elemental analyzer-continuous flow isotope ratio mass spectrometry: Chemical Geology, v. 192, p. 141–148.

Sun, S.S., and McDonough, W.F., 1989, Chemical and isotopic systematics of oceanic basalts: Implications for mantle composition and processes: Geological Society, London, Special Publications, v. 42, p. 313–345.

Sun, W.H., and Zhou, M.F., 2008, The ~860 Ma, Cordilleran-type Guandaoshan dioritic pluton in the Yangtze block SW China: Implications for the origin of Neoproterozoic magmatism: Journal of Geology, v. 116, p. 238–253.

Sun, W.H., Zhou, M.F., and Zhao, J.H., 2007, Geochemistry and tectonic significance of basaltic lavas in the Neoproterozoic Yanbian Group, southern Sichuan Province, southwest China: International Geology Review, v. 49, p. 554–571.

Sun, W.H., Zhou, M.F., Yan, D.P., Li, J.W., and Ma, Y.X., 2008, Provenance and tectonic setting of the Neoproterozoic Yanbian Group, western Yangtze block (SW China): Precambrian Research, v. 167, p. 213–236.

Tang, Q., Ma, Y., Zhang, M., Li, C., Zhu, D., and Tao, Y., 2013, The origin of Ni-Cu-PGE sulfide mineralization in the margin of the Zhubu mafic-ultramafic intrusion in the Emeishan large igneous province, SW China: Economic Geology, v. 108, p. 1889–1901.

Tang, Z.L., Yang J., Xu S., and Li W., 1992, Sm-Nd dating of the Jinchuan ultramafic rock body, Gansu: China Science Bulletin, v. 37, p. 1988–1991 (in Chinese).

Tao, Y., Li, C., Hu, R., Ripley, E.M., Du, A.D., and Zhong, H, 2007, Petrogenesis of the Pt-Pd mineralized Jinbaoshan ultramafic intrusion in the Permian Emeishan large igneous province, SW China: Contributions to Mineralogy and Petrology, v. 153, P. 321–337.

Tao, Y., Li, C., Song, X.Y., and Ripley, E.M., 2008, Mineralogical, petrological, and geochemical studies of the Limahe mafic-ultramafic intrusion and associated Ni-Cu sulfide ores, SW China: Mineralium Deposita, v. 43, p. 849–872.

Thakurta J., Ripley E.M., and Li C., 2008, Geochemical constraints on the origin of sulfide mineralization in the Duke Island Complex, southeastern Alaska: Geochemistry Geophysics Geosystems, v. 9, p. 3562–3585.

Tonnelier, N.J., 2010, Geology and genesis of the Jinchuan Ni-Cu-(PGE) deposit, China: Unpublished Ph.D. thesis, Sudbury, Laurentian University, p 192.

Walker, R.J., and Morgan, J.W., 1989, Rhenium osmium isotope systematics of carbonaceous chondrites: Science, v. 243, p. 519–522.

Wang, C.Y., Zhou, M.F., and Zhao, D., 2005, Mineral chemistry of chromite from the Permian Jinbaoshan Pt-Pd sulphide-bearing ultramafic intrusion in SW China with petrogenetic implications: Lithos, v. 83, p. 47–66.

Wang, C.Y., Zhou, M.F., Yang, S., Qi, L., and Sun, Y., 2014, Geochemistry of the Abulangdang intrusion: Cumulates of high-Ti picritic magmas in the Emeishan large igneous province, SW china: Chemical Geology, v. 378–379, p. 24–39.

Wasserburg, G.J., Jacobsen, S.B., DePaolo, D.J., McCulloch, M.T., and Wen, T., 1981, Precise determination of Sm-Nd ratios, Sm and Nd isotopic abundances in standard solutions: Geochimica et Cosmochimica Acta, v. 45, p. 2311–2323.

Xie, W., Song, X.Y., Deng, Y.F., Wang, Y.S., Ba, D.H., Zheng, W.Q., and Li, X.B., 2012, Geochemistry and petrogenetic implications of a Late Devonian mafic-ultramafic intrusion at the southern margin of the Central Asian orogenic belt: Lithos, v. 144, p. 209–230.

Xie, W., Song, X.Y., Chen, L.M., Deng, Y.F., Zheng, W.Q., Wang, Y.S., Ba, D.H., Yin, M.H., and Luan, Y., 2014, Geochemistry insights on the genesis of the subduction-related Heishan magmatic Ni-Cu-(PGE) deposit, Gansu,

northwestern China, at the southern margin of the Central Asian orogenic belt: Economic Geology, v. 109, p. 1563–1583.
Yan, D.P., Zhou, M.F., Song, H.L., and Fu, Z.R., 2003, Structural style and tectonic significance of the Jianglang dome in the eastern margin of the Tibetan plateau, China: Journal of Structural Geology, v. 25, p. 765–779.
Yang, G., Du, A.D., Lu, J.R., Qu, W.J., and Chen, J.F., 2005, Re-Os dating of the massive sulfide ores from the Jinchuan Ni-Cu-PGE deposit by ICPMS: Science in China Series D Earth Sciences, v. 48, p. 1672–1677 (in Chinese with English abstract).
Yang, S.H., Qu, W.J., Tian, Y.L., Chen, J.F., Yang, G., and Du, A.D., 2008, Origin of the inconsistent apparent Re-Os ages of the Jinchuan Ni-Cu sulfide ore deposit, China: Postsegregation diffusion of Os: Chemical Geology, v. 247, p. 401–418.
Zhang, M., Kamo, S.L., Li, C., Hu, P., and Ripley, E.M., 2010, Precise U-Pb zircon-baddeleyite age of the Jinchuan sulfide ore-bearing ultramafic intrusion, western China: Mineralium Deposita, v. 45, p. 3–9.
Zhang, Z.Q., Du, A., Tang, S., Lu, J., Wang, J., and Yang, G., 2004, Age of the Jinchuan copper-nickel deposit and isotopic geochemical feature of its source: Acta Geologica Sinica, v. 78, p. 359–365 (in Chinese with English abstract).
Zhang, Z.W., Tang, Q.Y., Li, C., Wang, Y., and Ripley, E.M., 2017, Sr-Nd-Os-S isotope and PGE geochemistry of the Xiarihamu magmatic sulfide deposit in the Qinghai-Tibet plateau, China: Mineralium Deposita, v. 52, p. 51–68.
Zhao, J.H., and Zhou, M.F., 2007a, Neoproterozoic adakitic plutons and arc magmatism along the western margin of the Yangtze block, South China: Journal of Geology, v. 115, p. 675–689.
——2007b, Geochemistry of Neoproterozoic mafic intrusions in the Panzhihua district (Sichuan Province, SW China): Implications for subduction-related metasomatism in the upper mantle: Precambrian Research v. 152, p. 27–47.
Zhao, X.F., Zhou, M.F., Li, J.W., Sun, M., Gao, J.F., Sun, W.H., and Yang, J.H., 2010, Late Paleoproterozoic to early Mesoproterozoic Dongchuan Group in Yunnan, SW China: Implications for tectonic evolution of the Yangtze block: Precambrian Research v. 182, p. 57–69.
Zhou, M.F., Kennedy, A.K., and Sun, M., 2002a, Neoproterozoic arc-related mafic intrusions along the northern margin of South China: Implications for the accretion of Rodinia: Journal of Geology, v. 110, p. 611–618.
Zhou, M.F., Yan, D.P., Kennedy, A.K., Li, Y.Q., and Ding, J., 2002b, SHRIMP U-Pb zircon geochronological and geochemical evidence for Late Proterozoic arc magmatism along the western margin of the Yangtze block, South China: Earth and Planetary Science Letters, v. 196, p. 51–67.
Zhou, M.F., Ma, Y., Yan, D.P., Xia, X., Zhao, J.H., and Sun M., 2006, The Yanbian terrane (southern Sichuan Province, SW China): A Neoproterozoic arc assemblage in the western margin of the Yangtze block: Precambrian Research, v. 144, p. 19–38.
Zhou, Y., Zhong, H., Li, C., Ripley, E.M., Zhu, W.G., Bai, Z.J., and Li, C., 2017, Geochronological and geochemical constraints on sulfide mineralization in the Qingmingshan mafic intrusion in the western part of the Proterozoic Jiangnan orogenic belt along the southern margin of the Yangtze craton: Ore Geology Reviews, v. 90, p. 618–633.
Zhu, W.G., Zhong, H., Deng, H.L., Wilson, A.H., Liu, B.G., Li, C.Y., and Qin, Y., 2006, SHRIMP zircon U-Pb age, geochemistry, and Nd-Sr isotopes of the Gaojiacun mafic-ultramafic intrusive complex, SW China: International Geology Review, v. 48, p. 650–668.
Zhu, W.G., Zhong, H., Li, X.H., Liu, B.G., Deng, H.L., and Qin, Y., 2007, $^{40}Ar/^{39}Ar$ age, geochemistry and Sr-Nd-Pb isotopes of the Neoproterozoic Lengshuiqing Cu-Ni sulfide-bearing mafic-ultramafic complex, SW China: Precambrian Research, v. 155, p. 98–124.
Zhu, W.G., Zhong, H., Li, X.H., Deng, H.L., He, D.F., Wu, K.W., and Bai, Z.J., 2008, SHRIMP zircon U-Pb geochronology, elemental, and Nd isotopic geochemistry of the Neoproterozoic mafic dykes in the Yanbian area, SW China: Precambrian Research, v. 164, p. 66–85.
Zhu, W.G., Li, X.H., Zhong, H., Wang, X.C., He, D.F., Bai, Z.J., and Liu, F., 2010, The Tongde Picritic Dikes in the western Yangtze block: Evidence for ca. 800 Ma mantle plume magmatism in South China during the breakup of Rodinia: Journal of Geology, v. 118, p. 509–522.
Zindler, A., and Hart, S.R., 1986, Chemical geodynamics: Annual Review of Earth and Planetary Sciences, v. 14, p. 493–571.

Jun-Hua Yao graduated from Henan Polytechnic University of China in 2013 and is now a Ph.D. candidate at the Institute of Geochemistry, Chinese Academy of Sciences. His research interests include the origin of mafic-ultramafic rocks and magmatic Cu-Ni sulfide deposits.